

A New Microchannel Heat Sink Design Using Porous Media Inserts

Hamdi E. Ahmed^{a*}, Issam M. Ali Aljubury^b, Ammar A. Farhan^c, Mohammed Gh. Jehad^a

^aDepartment of Mechanical Engineering, University of Anbar, 31001 Ramadi, Iraq

^bDepartment of Mechanical Engineering, University of Baghdad, 10071 Baghdad, Iraq

^cDepartment of Energy Engineering, University of Baghdad, 10071 Baghdad, Iraq.

Received 21 NOV 2021

Accepted 31 JAN 2022

Abstract

ACFD study is carried out to enhance the turbulent convection heat transfer of a solid plate-fin micro channel heat sink (MCHS). The goal of this study is to replace the solid fins with porous fins having a constant and variable cross-sectional area with the vertical and axial direction. Convergent and divergent porous fins are also explored. The effect of doubling the size of the porous fins is tested as only the foam is proposed to be above the heat sink substrate without channels. The FVM is adopted for solving the governing equations in 3D. Temperature-dependent properties of water are considered. The results are displayed in terms of the Nusselt number (Nu), wall temperature distribution, pressure drop, friction factor, hydraulic-thermal performance (JF), temperature contours, and wall temperature uniformity (TU). The results reveal that the maximum Nuis 21.0 times associated with a friction factor increase of 3.06 times compared to the traditional design. The highest JF is 15.87 for the MCHS-5 when $a = 1.0$ mm and $b = 0.0$ mm at $Re = 3000$. The non-uniform cross-sectional area of the porous fin shows a great thermal performance compared to the standard one. A slight increase in the Nu with high pressure drop penalty is shown when the porous media volume is doubled.

© 2022 Jordan Journal of Mechanical and Industrial Engineering. All rights reserved

Keywords: Porous media, MCHS, Turbulent flow, Hydraulic-thermal performance, Temperature-dependent fluid properties.

Nomenclatures

a	width of the fin base, m	TU	Temperature uniformity factor
A_c	heat transfer surface area, m ²	u	fluid velocity, m/s
b	width of the fin tip, m	W	substrate width, m
C	Inertia coefficient	x, y, z	x, y, z-coordinates
CF	Forchheimer factor	x^+, y^+, z^+	Criteria of mesh refinement
c_p	Specific heat capacity, J/kg·K	Greeks	
D_h	hydraulic diameter, m	α	Thermal diffusivity, m ² /s
d_e	Edge diameter of porous zone, m	J_ϕ	turbulent diffusion coefficient
d_p	Pore diameter, m	ε	turbulent energy dissipation rate, m ² /s ³
f	Friction factor	γ	Thermal conductivity, W/m·K
H	fin height, m	ρ	Fluid density, kg/m ³
h	Convection heat transfer coefficient, W/m ² ·K	ϵ	Porosity
JF	Hydro-thermal performance factor	μ	Dynamic viscosity, Pa·s
k	Turbulent kinetic energy, m ² /s ²	μ_e, μ_l, μ_t	effective, laminar, turbulent viscosity, Pa·s
K	Permeability, m ²	ϕ	transported scalar
L	length of the MCHS, m	Subscripts	
N	number of the heat sink channels	eff	effective
Nu	Nusselt number	f	fin
p	Pressure, Pa	f	fluid
Pr	Prandtl number	m	mean
q	Heat flux, W/m ²	p	porous
Re	Reynolds number	s	solid
S_ϕ	source term		
T	Temperature, K		

* Corresponding author e-mail: hamdi.ahmed@uoanbar.edu.iq.

1. Introduction

Recently, MCHS has received much attention due to the quick progress in microelectronic technology, the power density of electronic components is increasing continuously, which restricts their performance development. To ensure the electronic components operate safely and functionally, efficient thermal management techniques are critical and urgently required. The microchannel heat sink (MCHS) was introduced first by Tuckerman and Pease [1] in the 1980s and has become a promising alternative technique for heat rejection because it can remove a heat flux as high as 790 W/cm^2 . The MCHS has attracted a great deal of attention during the last three decades due to its wide thermal applications, convenient size, reliability, operating stability, and cooling efficiency [2, 3]. It is used for cooling microelectronic components, such as electric generators, microfluidic microbial fuel cells, heat exchangers in the automotive market, concentrator photovoltaic systems, and light-emitting diodes. Therefore, the MCHS is recognized as one of the most promising cooling techniques which offers high heat absorption from the chips. In the past decades, a lot of investigations were carried out experimentally and/or numerically to reduce the thermal resistance and pumping power of MCHS as they are considered as the two key issues for evaluating the hydraulic-thermal performance. [4–8]. The performance of these devices is directly related to the substrate temperature; therefore, it is a crucial issue to maintain the electronic equipment below the critical temperature [9]. Thermal resistance, cooling uniformity (Wall temperature distribution uniformity), and pressure drop (pumping power) are all critical metrics for MCHS [2, 10].

Metal foam is a particular kind of porous medium that can absorb a significant amount of heat from the solid through conducting and rejecting it to the fluid by convection. Metal foam shows different attractive features in comparison with its solid material counterparts. It has advantages, such as low volume, low density, high thermal conductivity, high effective heat transfer surface area, high flow-mixing capability, and low manufacturing cost. It is used in several thermal systems, such as heat exchangers, heat sinks, fuel cells, and solar collectors. It was shown that the use of metal foam insertion can enhance thermal performance significantly up to 40 times. The solid/fluid thermal conductivity was observed to be an important parameter to increase the heat dissipation by coolants. Researchers observed a high-pressure drop penalty accomplished to the thermal performance enhancement with the existence of metal foam [11–14].

The MCHS with metal foam insert increases both the surface contact area-to-volume ratio and local velocity mixing of the coolant, therefore, resulting in a better convective heat transfer rate. The thermal performance of such kinds of heat sinks can be improved by designing the configurations and porosity conditions properly, thus making the heat sink with porous insertion suitable for micro-size electronics cooling [15–18].

Hung et al. [15] investigated computationally the laminar hydraulic-thermal performances of MCHS by filling the channels with porous inserts in form of

rectangular, outlet enlargement, trapezoidal, thin rectangular, block, and sandwich distributions. It was noted that the trapezoidal porous distribution had thermal superiority at low Re number, while the rectangular porous distribution had thermal superiority at high Re number among other designs. The thermal performance was increased by using the porous inserts and also increased at a high Re number. A significant increase in the pressure drop was monitored when a porous medium was added to the channel. Hung et al. [19] explored numerically the laminar hydraulic and thermal performance of MCHS by enlarging the channel outlet using a porous insertion. It was demonstrated that increasing the width or height enlargement ratio could reduce the pressure drop across the channel. An enhancement in the Nusselt number and temperature control effectiveness and a reduction in the thermal resistance was observed. They stated that improving the hydraulic and thermal performance of the MCHS might be significantly obtained. A remarkable increase in the pressure drop was displayed across the MCHS by using the porous insertion.

Li et al. [10] investigated the thermal management of high-powered electronic components by inserting a metal foam in pin-fin hybrid heat sinks numerically. Their proposed design could enhance the heat transfer more than the metal foam heat sink and the pin-fin heat sink. They attributed this improvement to the increase in heat conduction and heat convection. They found that the heat transfer of the proposed design was more influenced by the foam porosity, whilst the pressure drop was affected by the pore size. Their results demonstrated that the thermal performance ratio of the proposed design was 1.6 times more than the traditional pattern. Seyf and Layeghi [20] studied the laminar thermal performance of an elliptical pin-fin heat sink with and without metal foam inserts numerically. It was indicated that the structural properties of porous media insert could considerably affect the frictional loss and heat transfer of the heat sink. An increase in the Nusselt number by 400% in some cases could be achieved by reducing the porosity and increasing the Re number (particularly at low Re number). An increase in the pressure drop was displayed with decreasing permeability and increasing the Re number.

Chuan et al. [8] modified the design of the MCHS by utilizing porous fins instead of solid fins to reduce the pressure drop across the heat sink. They found that the pressure drop was decreased by 47.9% lower than the traditional one while only an increment of 5% was recorded in the thermal resistance. They stated that the use of porous fins could cause a non-zero velocity of coolant at the interface between the channel and porous fin in which the coolant might behave like a “slip” on the channel wall. Chen [9] analyzed the laminar forced convection heat transfer in MCHS by considering the MCHS as a fluid-saturated porous medium due to the small dimensions of the microstructures. They found that the solid temperature distribution was unaffected by the fluid inertia force and the channel aspect ratio, while the dimensionless velocity distribution and the fluid temperature distribution relied on the inertial force parameter and the aspect ratio. The Nu number was increased with increasing the aspect ratio and porosity, whereas it was decreased with increasing the effective thermal conductivity ratio. Less effect of the

inertial force on the mean fluid temperature and the Nu number was found.

Li et al. [2] proposed an improved design of double-layer MCHS having high thermal performance and low frictional loss using porous media insertion under the laminar flow regime. They compared the thermal performance of four patterns; solid-fins single layer, porous-fins single layer, solid-fins double layer, and porous-fins double-layer MCHS. Their numerical results inferred that the porous fins upper layer and solid fins lower layer showed the lowest thermal resistance and best channel wall temperature uniformity among others at the corresponding Re number. A lower pressure drop of porous fins in the double-layered MCHS played a key role in the thermal performance enhancement. Ghahremannezhad et al. [3] accomplished a numerical comparison between the thermal-hydraulic performance of solid-plate-fin and porous-plate-fin double-layered MCHS. They could obtain higher thermal-hydraulic performance. The pumping power and thermal resistance could be minimized by optimizing the porous media parameters. Changing the porous fin thickness could increase the heat transfer rate. The superiority of their proposed pattern was verified with different porosities of substrates and MCHS materials. Wang et al. [4] explored the performance of a porous-ribs double-layer MCHS numerically. The upper layer was porous media fins while the lower layer was solid fins. It was revealed that not only the cooling performance was remarkably increased, but around 14.06%, also the consumption of the pumping power was also noticeably decreased by 16.40% in comparison with the traditional one. The optimized model showed more substrate temperature uniformity and lower than the baseline pattern. Arasteh et al. [11] enhanced the hydrothermal performance of the double-layered heat sink by using a porous sinusoidal fin under the laminar flow regime. At the optimum porous thicknesses, nanofluid was employed to enhance the heat sink thermal performance. By varying the porous thickness, the optimum porous thickness was obtained. The maximum hydraulic-thermal performance was 2.12.

Feng et al. [21] implemented an experimental and numerical study on finned metal foam and metal foam heat sinks having different heights subjected under impinging air jet cooling. Their final results exhibited that for the corresponding Re number, the heat dissipation of the metal foam heat sink increased monotonously when the foam height decreased, whilst the heat transfer increased first and then slightly decreased for the finned metal foam heat sink. For the same pumping power, the heat transfer of the metal foam heat sink was unaffected by the foam height whereas it increased with increasing the foam height for the other pattern. It was reported that the heat transfer of the finned metal foam heat sink outperformed the other pattern by about 1.5–2.8 times for the corresponding having the same height. Siavashi et al. [22] studied numerically the fluid flow and heat transfer of impinging jet flow through a cylindrical porous heat sink. They have found that the decrease in the ratio of (height/diameter) of the heat sink could increase the heat transfer rate.

Deng et al. [23] carried out a comparative study between an analytical solution and 3D numerical simulation to show the effect of insertion of porous media

in a MCHS. They found that the fin-averaged temperature was lower than the channel-averaged temperature near the bottom of the channel. The maximum substrate thickness was obtained with a low convective thermal resistance.

Yerramalle et al. [24] studied numerically a flow across a channel filled partly with cylindrical porous medium under three hydro-dynamic interface conditions which were; the slip condition, the stress continuity condition, and the stress jump condition. They concluded that their numerical simulation model was better for predicting the velocity profile in the fluid zone, the velocity profile was close to the interface, and the thickness of the boundary layer was compared to the analytical solution. A rectangular channel filled with an open-cell metal foam and exposed to constant asymmetrically heat flux was studied experimentally by Arbak and Dukhan [25] to examine the forced convection heat transfer characteristics. It was shown that the channel filled with metal foam has a Colburn factor greater than that of the empty channel by 407%.

A flow through a micro-channel partly filled with a porous medium was studied analytically by Xu et al. [26] to investigate its effect on the force convective heat transfer. They obtained an exact solution for the velocity profile inside the micro-channel. Also, it was reported that the friction factor was reduced with the growth of the Darcy number. Xu et al. [27] investigated numerically the performance of convection heat transfer performance in metal-foam heat exchanger assuming local thermal equilibrium and non-equilibrium models. It was found that the Nusselt number with the local thermal equilibrium model was greater than that with the local thermal non-equilibrium model.

AL-Migdady et al [28] performed a numerical analysis on the cooling performance of phase change material-based heat sinks with Aluminum foam. While keeping the heat flux input constant, two different PCMs and three distinct coefficients of convective heat transfer values were investigated. Comparing with the non-metal foam, the aluminum foam insertion of 0.97 and 0.90 porosity resulted in a base temperature drop of 5 and 6°C, respectively. Alshare et al. [29] conducted a steady-state two-dimensional developing flow in a wavy microchannel heat sink. It was discovered that as the Knudsen number increased, the slip velocity and temperature jump raised. It has been demonstrated that raising the wave amplitude could increase the heat transfer rate associated with increasing the frictional losses.

From the review of the open literature, and based on the best knowledge of the authors, it is shown that very few numerical studies are published on using porous fins instead of solid fins in the MCHS. In addition, no paper studied the effect of using variable cross-sectional area of the porous fins on the thermal and hydraulic flow characteristics. Based on the advantages of the porous media, it is expected that the convection heat transfer surface area of the porous fin will be greater and the flow path will be longer due to the fluctuation flow through the pores of the porous media compared to the solid fin. In addition, higher pressure drop penalty is also expected, thus, it is worth asking whether the hydraulic-thermal performance will be greater than one or not. The present work aims to fill this research gap with the main objective

to investigate numerically, in three-dimensions, the impact of using porous fins having a constant or changeable cross-section with the vertical and axial direction. Different geometric parameters of porous fins are examined considering the volume of the porous media constant along the tests. The results have been displayed in terms of the Nusselt number, wall temperature, friction factor, pressure drop, hydraulic-thermal performance, temperature uniformity factor, and temperature contours and then interpreted and analyzed in detail.

2. Computational model

2.1. Model description

The domain of the computational model of an aluminum plate-fin micro-channel heat sink in which single-channel is investigated here as illustrated in Figure 1(A). The substrate width (W) and length (L) are 1 mm, and 10 mm, respectively as depicted in Figure 1(B). The height (H) of the fin is 2 mm. Thus, the height of the base of the heat sink substrate is $H/2$ and the width of the channel is $W/2$. The width of the fin is identical to the width of the flow channel. There are the channel number (N) and the number of fins ($N+1$). The hydraulic diameter is taken for the fluid zone only when the fin is solid, whilst the hydraulic diameter is doubled for the fluid and fin zones when the fin is porous media. The inlet and outlet boundary conditions are the velocity and pressure applied

at the entrance and exit of the channel, respectively. The lateral sides of the fluid domain are considered as a symmetry boundary condition. Constant heat flux is applied to the base of the substrate. The traditional MCHS is taken as a baseline case for comparing other proposed patterns to show their superiority. Therefore, the baseline pattern is denoted by MCHS-0 in this paper

2.2. Patterns and variables

Several variable parameters are investigated here for obtaining different heat sink patterns to enhance the thermal and hydraulic performance of the MCHS. The traditional pattern considered in this study is the plate-solid fin microchannel heat sink denoted by MCHS-0 and cooled by water. The first proposed design is a pattern of an aluminum porous fin with a fluid zone denoted by MCHS-1 as seen in Figure 2(A). The second pattern is using a solid fin with a porous zone (i.e., instead of the pure fluid core) denoted by MCHS-2, see Figure 2(B). The third is using a porous fin with a width of 1 mm instead of 0.5 mm while the height is 1 mm instead of 2 mm and the zone of the fluid is above the porous zone (middle porous fin with the upper fluid zone), MCHS-3, Figure 2(C). The fourth is using porous fin with porous zone, MCHS-4, Figure 2(D). The total fin volume of all the above patterns is maintained constant throughout the comparison tests.

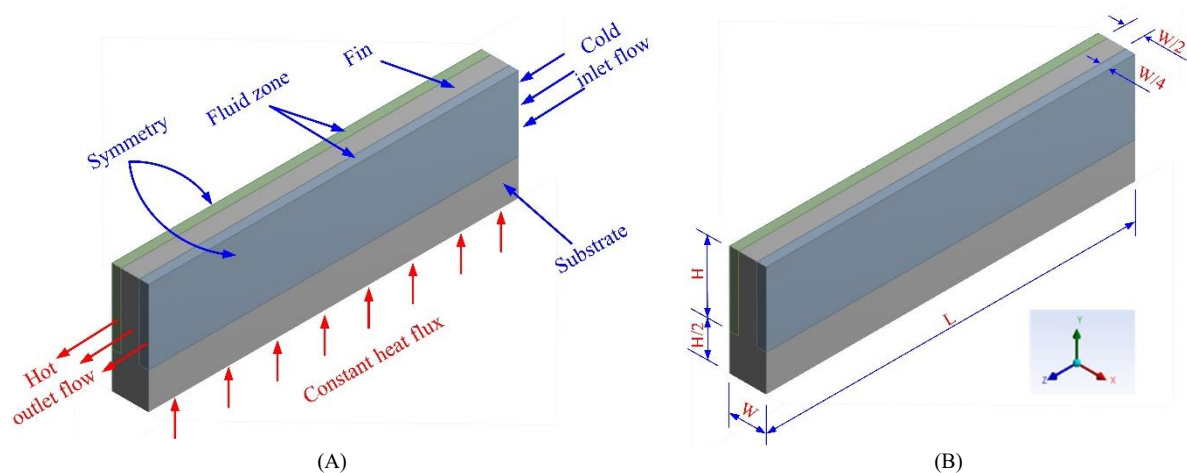


Figure 1. Schematic diagram of (A) the computational domain of the physical problem MCHS-0, and (B) geometric parameters.

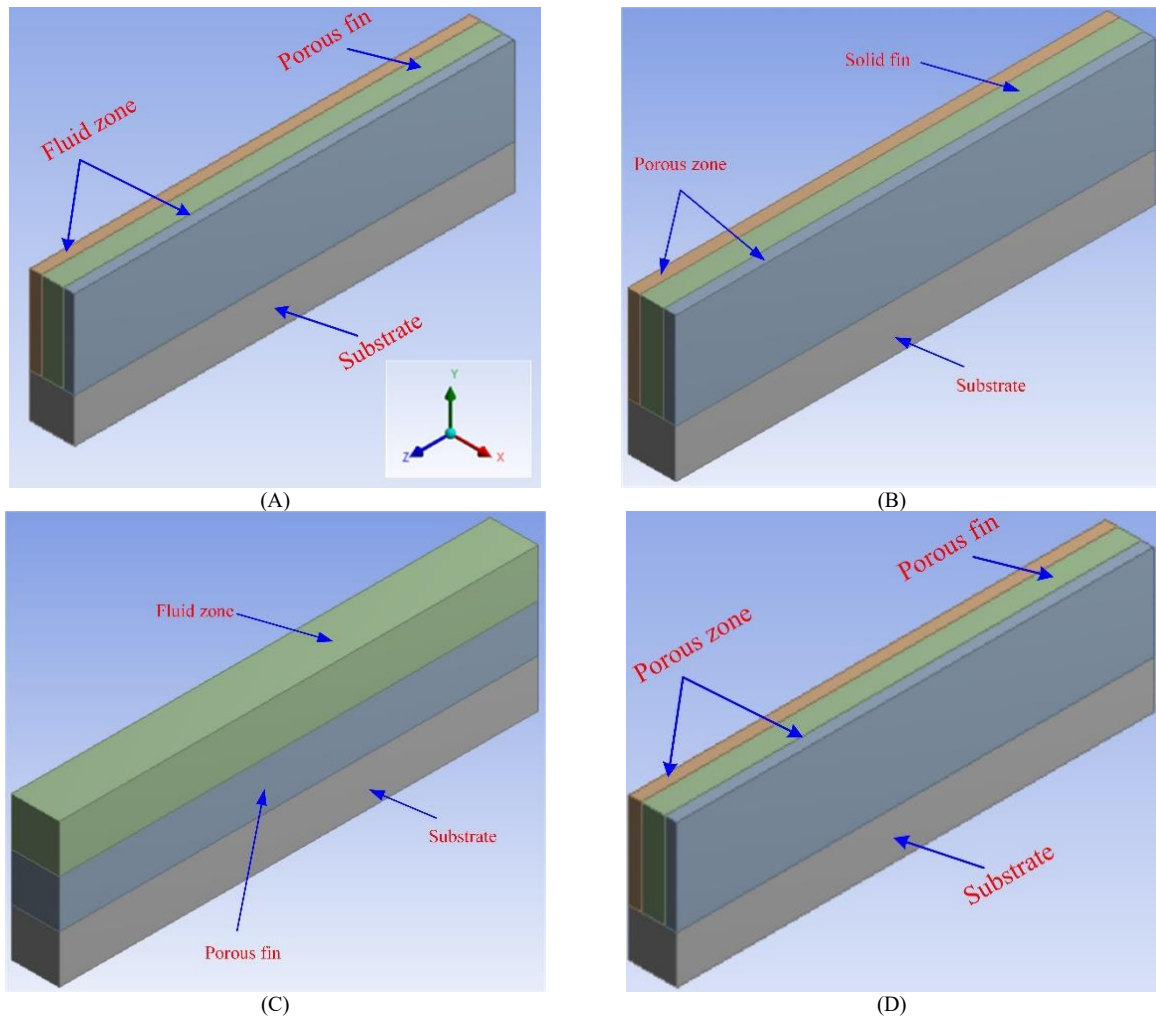


Figure 2. The patterns considered in the current study;

(A) Porous fin-pure fluid zone, MCHS-1, (B) solid fin-porous zone, MCHS-2, (C) middle porous fin-upper fluid core MCHS-3, and (D) porous fin-porous zone, MCHS-4.

The pattern of MCHS-1 is further studied by varying the parameters a and b as shown in Figure 3(A). The cuboidal fin is replaced by a trapezoidal one in which the cross-sectional area of the fin is varied with the y -axis. This pattern is denoted by MCHS-5. It is worth to be mentioned that the total volume of the fins is the same. Four values for each a and b are investigated and analyzed to show their superiority in heat dissipation. These parameters are tabulated in Table 1. Further design for the porous fin is proposed here in which the cross-sectional area of the porous fin is varied with the longitudinal flow direction (z -axis). In the current situation, two patterns can be obtained; an upstream end apex-angle porous fin which is denoted by MCHS-6, and a downstream end apex-angle porous fin which is denoted by MCHS-7, as illustrated in Figure 3(B), and (C), respectively. Divergent foam fin with axial direction, MCHS-8, as seen in Figure 3(D), and convergent foam fin with axial direction, MCHS-9, as seen in Figure 3(E), are also investigated. In this style of the fin, the effect of the thermal boundary layer in the porous zone is concerned to emphasize that the uniform fin volume is not an effective and economical design. It should be

mentioned that the volume of the fin is kept constant to investigate its effect on the conductive heat transfer between the fin and substrate and the convective heat transfer between the fluid and porous media. All the above patterns are abbreviated in Table 2 for more clarification and simplification.

Table 1. Variable parameters and dimensions of the fin geometry.

No.	Variables		Fin shape
	a (mm)	b (mm)	
1.	0.5	0.5	Cuboidal cross-section normal to flow direction
2.	0.7	0.3	Trapezoidal cross-section normal to flow direction
3.	0.8	0.2	Trapezoidal cross-section normal to flow direction
4.	1.0	0.0	Triangular cross-section normal to flow direction

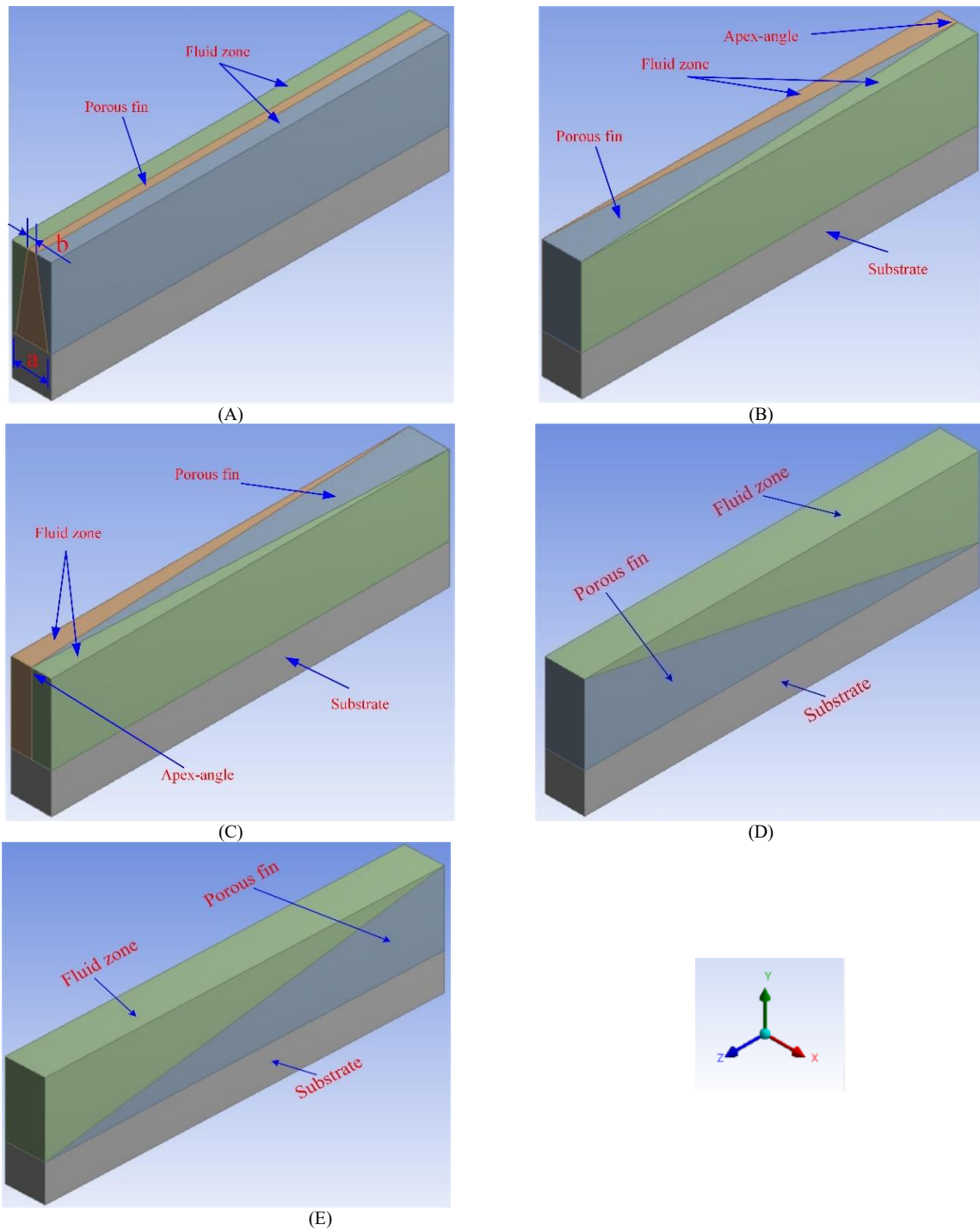


Figure 3. Schematic diagram of (A) geometric parameters of the trapezoidal porous fin- fluid zone, MCHS-5, (B) upstream apex-angle porous fin, MCHS-6, (C) downstream apex-angle porous fin, MCHS-7, (D) divergent fin with axial direction, MCHS-8, and (E) convergent fin with axial direction, MCHS-9.

Table 2. Abbreviation of all MCHS patterns proposed in this study.

No.	Patterns	Abbreviation
1	Traditional plate-fin MCHS	MCHS-0
2	Porous fin-pure fluid zone MCHS	MCHS-1
3	Solid fin-porous zone MCHS	MCHS-2
4	Middle porous fin-upper fluid zone MCHS	MCHS-3
5	Porous fin-porous zone MCHS	MCHS-4
6	Porous fin with cross-sectional area varied with y-axis MCHS	MCHS-5
7	Upstream end apex-angle porous fin MCHS	MCHS-6
8	Downstream end apex-angle porous fin MCHS	MCHS-7
9	Divergent foam fin with axial direction	MCHS-8
10	Convergent foam fin with axial direction	MCHS-9

3. Numerical approach

Computational fluid dynamics (CFD) is utilized for estimating the velocity, pressure, and temperature in the microchannel heat sink. The numerical simulation, using ANSYS-Fluent v.14, is carried out by solving the governing equations along with the boundary conditions using the finite volume method (FVM). The equations of the solid and fluid domain are solved simultaneously as a single domain conjugate problem. The flow field is solved by using the SIMPLE algorithm. The implicit method is adopted for discretizing the governing equations. Both the diffusion term and convective terms in the momentum and energy conservation equations are discretized by the second-order upwind differencing scheme. In addition, the second-order upwind differencing scheme is used for approximating the turbulent kinetic energy and turbulent dissipation rate. The solutions are considered to be converged when the normalized residuals of all variables become negligible (less than 1×10^{-6}) and the velocity components become unchangeable.

3.1. Boundary conditions

The following boundary conditions are assumed in the numerical computation. It is worth to be mentioned that owing to the symmetry, the flow through a single row of the fin is simulated.

- i. A heat flux of 300 kW/m^2 is applied to the bottom of the substrate base. The maximum temperature difference between the wall temperature and inlet bulk temperature does not exceed 37.7 K .
- ii. Uniform velocity profile is assumed at the channel inlet ranged depending on the value of Reynolds number which is varied from 2000 to 6000. The inlet fluid temperature is 300 K .
- iii. An outlet pressure condition is applied at the channel exit in which the gauge pressure equal to zero. The temperature gradient is zero ($\frac{dT}{dz} = 0$).
- iv. No-slip boundary condition is assumed at the solid walls which are in contact with the fluid, and the heat flux is conserved ($\gamma_s \frac{dT_s}{dn} = \gamma_f \frac{dT_f}{dn}$).
- v. The symmetry boundary condition is applied on the right and left surfaces of the domain.
- vi. An adiabatic and no-slip boundary conditions are applied on the other walls.

The temperature-dependent thermophysical properties of water are considered and presented in Table 3 where the temperature is in K. The values of the water properties are correlated from the data reported in [30]. The properties of the aluminum are 2702 kg/m^3 for the density, 237 W/m K for the thermal conductivity, and 903 J/kg K for the specific heat capacity. The current simulations are carried out at fixed porosity of 0.93, 10PPI, the permeability of $1.47523 \times 10^{-7} \text{ m}^2$, Forchheimer factor of 0.060, and inertia coefficient of 156.49 m^{-1} .

The permeability is estimated by the following formula[31]

$$K = d_p^2 \times 73 \times 10^5 \times (1 - \epsilon)^{-0.0224} \times \left(\frac{d_e}{d_p}\right)^{-1.11} \quad (1)$$

where d_p and d_e are the pore size and edge diameter, respectively, which are estimated from the following formulas[31]

$$d_p = 0.0254 \times (PPI)^{-1} \quad (2)$$

$$d_e = 1.18 \times \left(\frac{1}{1 - e^{-\frac{1-\epsilon}{0.04}}}\right) \times \left(\frac{1-\epsilon}{3\pi}\right)^{1/2} \quad (3)$$

The Forchheimer factor (CF) and the inertia coefficient (C) are, respectively, determined by [31]

$$CF = 29.613 \times \left[\frac{(1-\epsilon)^{1.5226}}{d_p}\right] \times \sqrt{K} \quad (4)$$

$$C = \frac{CF}{\sqrt{K}} \quad (5)$$

The effective thermal conductivity of the fluid-filled with porous media is simply estimated by[4, 31]

$$\gamma_{\text{eff}} = \epsilon \gamma_f + (1 - \epsilon) \gamma_s \quad (6)$$

3.2. Assumptions

The sintered porous media is assumed isotropic, homogeneous, and fully saturated with the working fluid. Three-dimensional, incompressible, turbulent, and steady fluid flow is considered. Temperature-dependent thermophysical fluid properties are adopted and the gravity, body forces, and radiation effects are negligible. The heat sink is insulated from the outside environment. The solid surface and the working fluid are assumed to be in local-thermal-equilibrium throughout the porous region. Forchheimer-Brinkman-Darcy equation based on a volume-averaging method is used to model the fluid flow through a porous region [32–37].

3.3. Governing equations

Based on the above assumptions, the RNG $k-\epsilon$ turbulence model is adopted, due to its high accuracy and reliability for a wide class of flows particularly for low-Reynolds number and its possibility to generate quick changes, for solving the governing equations. The continuity, momentum, and energy conservation equations can be written in a general formula:

Continuity equation:

$$\frac{\partial}{\partial x}(\rho u \phi) + \frac{\partial}{\partial y}(\rho v \phi) + \frac{\partial}{\partial z}(\rho w \phi) = \frac{\partial}{\partial x} \left[\Gamma_\phi \frac{\partial \phi}{\partial x} \right] + \frac{\partial}{\partial y} \left[\Gamma_\phi \frac{\partial \phi}{\partial y} \right] + \frac{\partial}{\partial z} \left[\Gamma_\phi \frac{\partial \phi}{\partial z} \right] + S_\phi \quad (7)$$

Table 3. Temperature-dependent thermophysical properties of water.

Quantity	Unit	Polynomial correlation
k	W/m K	$-0.8185 + 7.86 \times 10^{-3}T - 1.03 \times 10^{-5}T^2$
ρ	Kg/m ³	$754.930 + 1.8898T - 3.62 \times 10^{-3}T^2$
μ	Pa s	$0.02466 - 1.3973 \times 10^{-4}T + 2.01 \times 10^{-7}T^2$
c_p	J/kg K	$5491.909 - 8.3940T + 1.34 \times 10^{-2}T^2$

The equations of the flow region and the metal foam region are tabulated in Table 4 and Table 5, respectively.

Table 4. Summary of equations solved for the fluid zone (eq. 5).

Equation	ϕ	Γ_ϕ	S_ϕ
Continuity	1	0	0
x-momentum	u	μ_e	$-\frac{\partial P}{\partial x} + \frac{\partial}{\partial x} \left[\mu_e \frac{\partial u}{\partial x} \right] + \frac{\partial}{\partial y} \left[\mu_e \frac{\partial v}{\partial x} \right] + \frac{\partial}{\partial z} \left[\mu_e \frac{\partial w}{\partial x} \right]$
y-momentum	v	μ_e	$-\frac{\partial P}{\partial y} + \frac{\partial}{\partial x} \left[\mu_e \frac{\partial u}{\partial y} \right] + \frac{\partial}{\partial y} \left[\mu_e \frac{\partial v}{\partial y} \right] + \frac{\partial}{\partial z} \left[\mu_e \frac{\partial w}{\partial y} \right]$
z-momentum	w	μ_e	$-\frac{\partial P}{\partial z} + \frac{\partial}{\partial x} \left[\mu_e \frac{\partial u}{\partial z} \right] + \frac{\partial}{\partial y} \left[\mu_e \frac{\partial v}{\partial z} \right] + \frac{\partial}{\partial z} \left[\mu_e \frac{\partial w}{\partial z} \right]$
Energy	T	$\frac{\mu_e}{\sigma_T}$	0
Turbulent Kinetic energy	k	$\mu_l + \frac{\mu_t}{\sigma_k}$	$-\rho \epsilon + G$
Turbulent dissipation	ϵ	$\mu_l + \frac{\mu_t}{\sigma_\epsilon}$	$\frac{\epsilon}{k} (c_1 G - c_2 \rho) \epsilon$

$$\text{where } G = \mu_t \left\{ 2 \times \left[\left(\frac{\partial u}{\partial x} \right)^2 + \left(\frac{\partial v}{\partial y} \right)^2 + \left(\frac{\partial w}{\partial z} \right)^2 \right] + \left[\frac{\partial u}{\partial y} + \frac{\partial v}{\partial x} \right]^2 + \left[\frac{\partial v}{\partial z} + \frac{\partial w}{\partial y} \right]^2 + \left[\frac{\partial u}{\partial z} + \frac{\partial w}{\partial x} \right]^2 \right\}$$

$$\mu_e = \mu_l + \mu_t$$

Table 5. Summary of equations solved for metal foam zone (eq. 5).

Equation	ϕ	Γ_ϕ	S_ϕ
Continuity	1	0	0
x-momentum	u	μ_l	$-\epsilon^2 \frac{\partial P}{\partial x} + (\epsilon - 1) \mu_l \left[\frac{\partial^2 u}{\partial x^2} + \frac{\partial^2 u}{\partial y^2} + \frac{\partial^2 u}{\partial z^2} \right] - \rho \epsilon^2 uv \frac{\partial}{\partial y} \left[\frac{1}{\epsilon} \right] - \frac{\mu_l}{K_p} \epsilon^2 u$ $-\rho F U \epsilon^2 u$
y-momentum	v	μ_l	$-\epsilon^2 \frac{\partial P}{\partial y} + (\epsilon - 1) \mu_l \left[\frac{\partial^2 v}{\partial x^2} + \frac{\partial^2 v}{\partial y^2} + \frac{\partial^2 v}{\partial z^2} \right] - \rho \epsilon^2 vv \frac{\partial}{\partial y} \left[\frac{1}{\epsilon} \right] - \frac{\mu_l}{K_p} \epsilon^2 v$ $-\rho F U \epsilon^2 v$
z-momentum	w	μ_l	$-\epsilon^2 \frac{\partial P}{\partial z} + (\epsilon - 1) \mu_l \left[\frac{\partial^2 w}{\partial x^2} + \frac{\partial^2 w}{\partial y^2} + \frac{\partial^2 w}{\partial z^2} \right] - \rho \epsilon^2 ww \frac{\partial}{\partial y} \left[\frac{1}{\epsilon} \right] - \frac{\mu_l}{K_p} \epsilon^2 w$ $-\rho F U \epsilon^2 w$
Energy	T	$\frac{\alpha_p}{\rho}$	0

$$\text{where } |U| = (u^2 + v^2 + w^2)^{1/2}$$

4. Validation of the simulation

The present computational modeling is validated with the experimental data and numerical results reported by Feng et al. [21]. In their work, an aluminum heat sink has a base area of 68×68 mm² and a thickness of 4 mm with an aluminum metal foam having a height of 30 mm attached to the upper surface of the substrate. The heat was supplied to the base of the heat sink in which the maximum difference between the base wall temperature and inlet bulk temperature did not exceed 50 K. Air inlet impinging circular tube was attached to the upper surface of the metal foam for jetting the air and air exits from two sides of the heat sink whilst the other two sides were considered adiabatic. The airflow rate range was from 3000 to 12,000 Reynolds number. The properties of the metal foam were; 0.963 porosity, 8 PPI, 3.142×10⁻⁷ m² permeability, and 0.0492 form drag coefficient. From above, the physical domain of Feng and his group is modeled and the results of the pressure drop and Nusselt number are depicted and compared as shown in Figure 4(A) and (B), respectively. The figure shows an acceptable matching between the present predicted results and their experimental and

numerical data. Further validation is carried out with the experimental data published by Wang et al. [38]. An aluminum heat sink having 8 fins (30 mm in-height) filled with a copper metal foam inserted in heat sink channels. The porosity, permeability, and inertia coefficient of the metal foam are 0.919, 1.298×10⁻⁰⁷ m², and 0.05919, respectively, for the range of Reynolds number of 2000–8000. The k - ϵ , renormalized group turbulence model is adopted in the current simulation with the consideration of the scalable wall functions for the near-wall treatment. The mesh is refined in the fluid domain near the walls attached to the fluid taking the distance between the first cell centroid and the wall as 0.05 mm. The deviation of the pressure drop can be attributed to the fact that, in their experiments, the inlet pressure tab was positioned after the fan immediately and the outlet pressure tab was at the exit of the channel. Therefore, the pressure drop was greater in their measurements as the deviation is about 38% as shown in Figure 4(C). An acceptable agreement is observed in the Nusselt number as depicted in Figure 4(D). Thus, the present CFD modeling can be safely depended on to predict the heat transfer and fluid flow through a plate-fin heat sink having solid and/or porous media.

5. Mesh independency test

The computational domain of all patterns investigated here is meshed using hexahedral cells as shown in Figure 5(A), (B). Uniform and structural mesh are being generated and no refinement is used near the wall because the y^+ value is satisfied in the whole domain, not just near the wall. As shown in Figure 5(B), only the apex-angle of the porous fin is meshed using tetrahedral elements due to

its sharp edge. All the zones are formed as a new single part in the design modeler of ANSYS to match the mesh nodes between each two contact zones in which high-quality mesh could be obtained. The maximum, minimum, and average mesh quality obtained are 1, 0.036, and 0.987, respectively, for the pattern of MCHS-7, for instance, in which the lowest mesh quality is observed. Whereas the mesh quality of the rest patterns is, respectively, 0.9999, 0.9999, and 1.

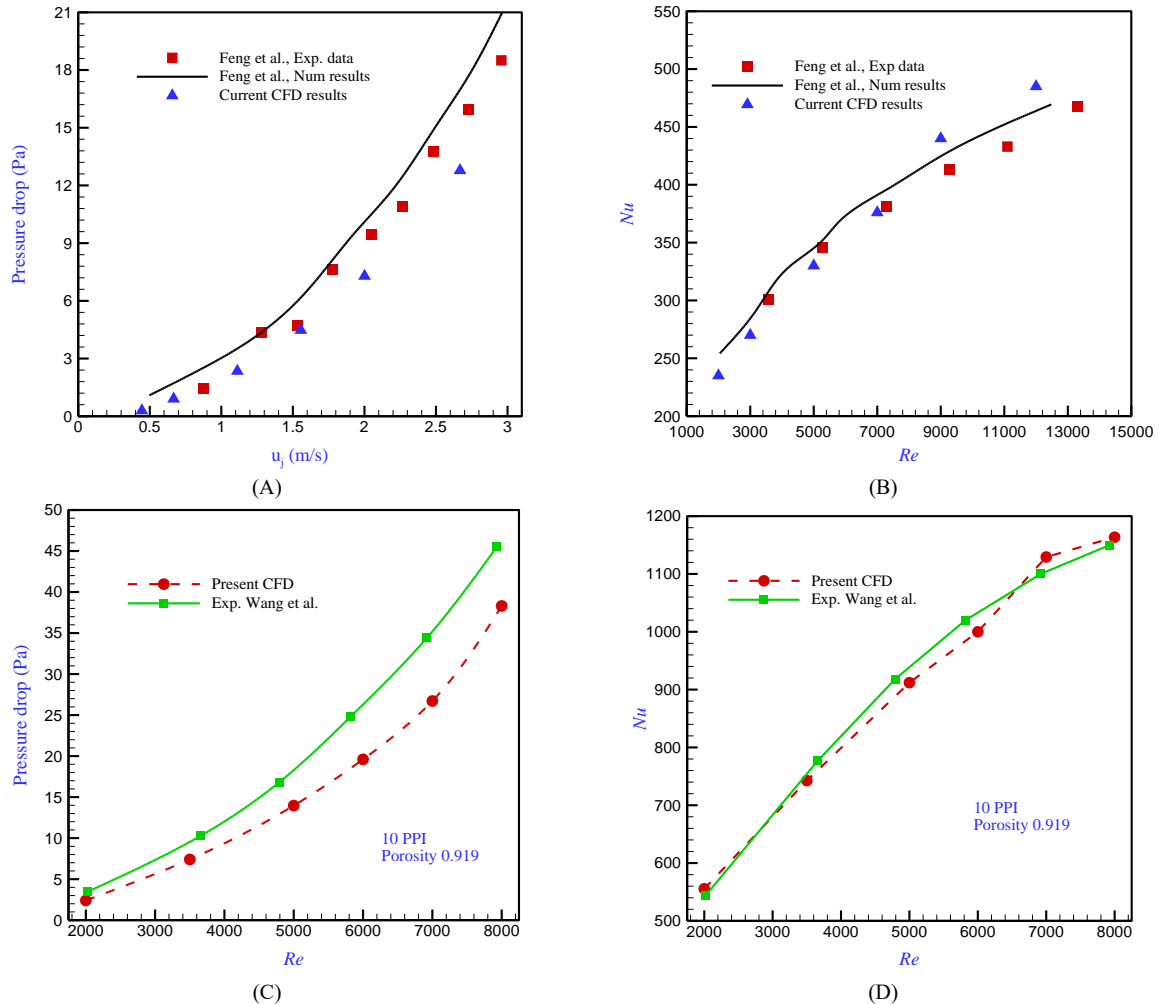


Figure 4. Validation with experimental and numerical results reported by Feng et al. [21], and Wang et al., [38]; (A) average pressure drop, (B) average Nusselt number, (C) pressure drop, and (D) average Nusselt number.

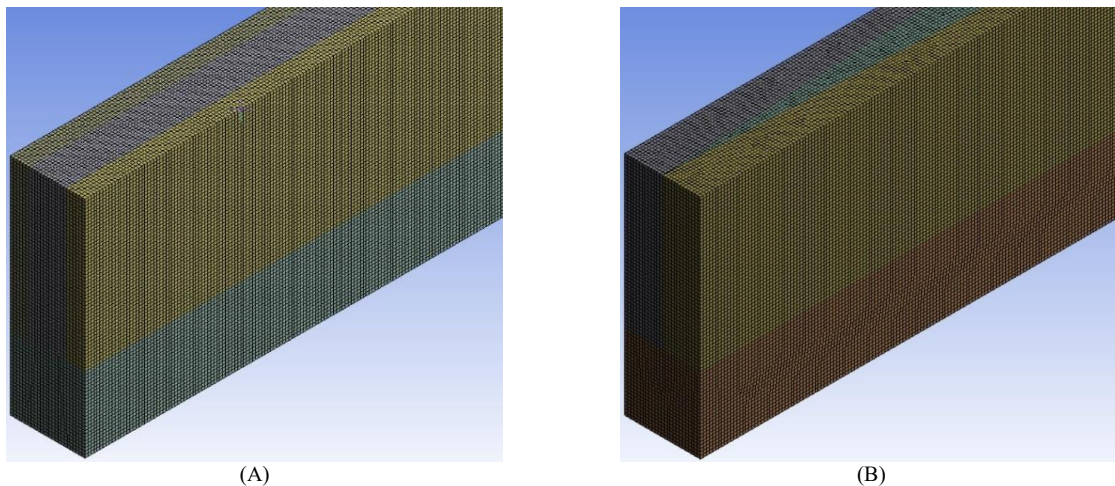


Figure 5. Meshing of the physical domain when the cross-sectional area of the fin and fluid zone is; (A) uniform, and (B) variable with the axial direction.

An extensive grid testing is carried out to guarantee grid independence. The tests are carried out at the highest value of the Reynolds number to make sure that the distance between the center of the first cell and the channel wall satisfies the value of y^+ . Different numbers of grid elements are tested as tabulated in Table 6. The axial pressure drop, outlet velocity profile, axial wall temperature distribution, and local Nusselt number are depicted with the mesh density as displayed in Figure 6(A)–(D). It is clear that the mesh density having an element size of 0.04 mm (i.e., the distance from the center of the first cell to the wall surface is 0.02 mm) is adequate and could provide accurate results in a shorter time compared to the finer one. The distance between the first cell center and the channel wall is estimated from y^+ in which the last is taken 10. This value of y^+ is fine enough due to the low turbulent Reynolds numbers covered in this

study. It should be mentioned that the domain is meshed uniformly and the x^+y^+ and z^+ are the same for any given near-wall cell.

Table 6. Nodes distribution in x -, y -, z -direction, and the total element number.

No.	Element size	node number			Total element number
	(mm)	x	y	z	
1.	0.1	10	30	100	33,000
2.	0.08	13	38	125	61,750
3.	0.06	17	50	167	141,950
4.	0.05	20	60	200	240,000
5.	0.04	25	75	250	468,750
6.	0.038	26	79	263	560,979

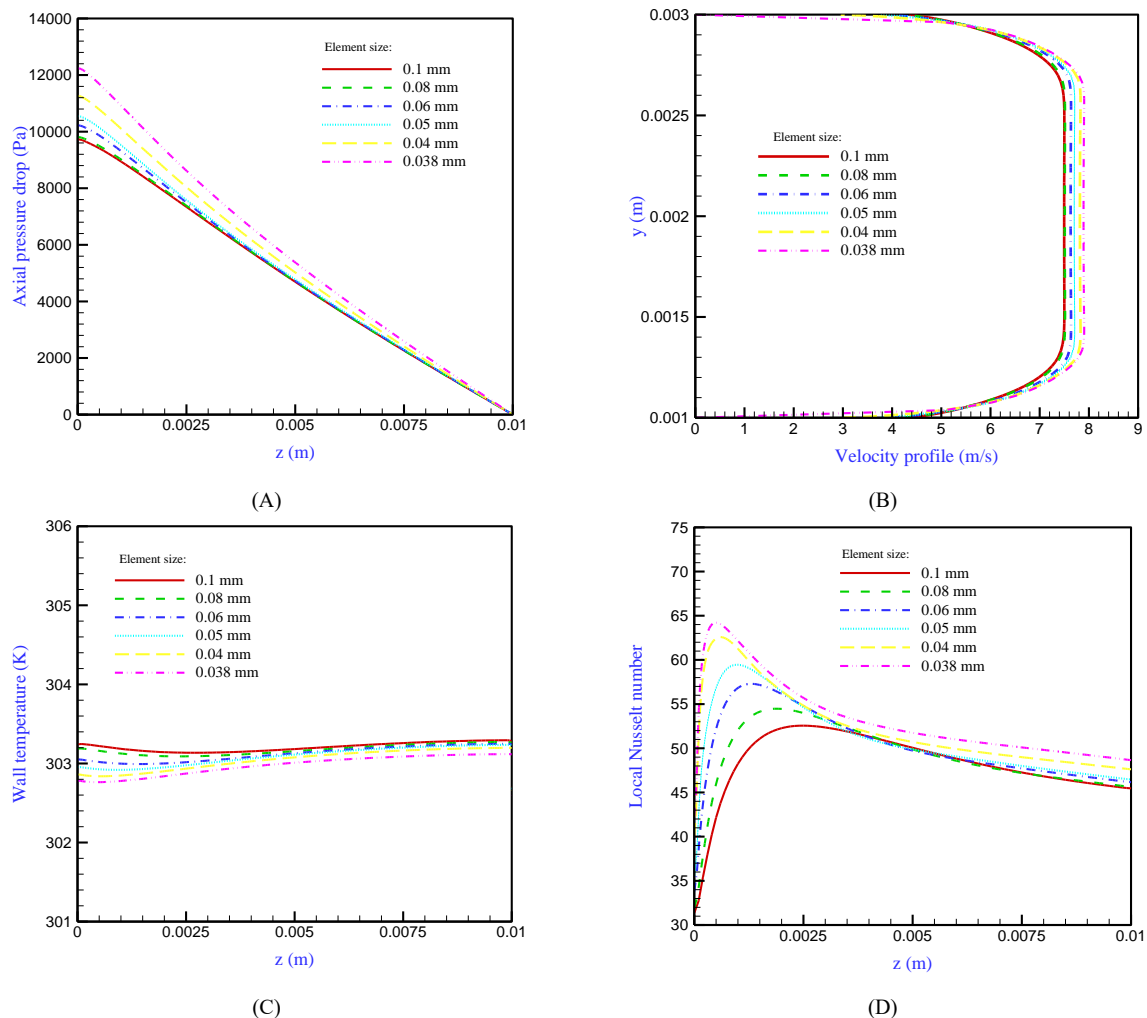


Figure 6. Quantities variation with the grid density; (A) axial pressure drop, and (B) velocity profile at the channel exit, (C) axial temperature distribution, and (D) local Nusselt number.

6. Data acquisition

The parameters estimated in the pre-processing such as the Reynolds number and post-processing, such as the Nusselt number, friction factor, and the hydraulic-thermal performance factor (JF) are interesting. The mean inlet water velocity is calculated by [30]

$$u_m = \frac{Re \mu}{\rho D_h} \quad (8)$$

where ρ , u_m , D_h , and μ represent, respectively, the fluid density, mean inlet fluid velocity, hydraulic diameter of the microchannel, and fluid kinematic viscosity. There are two hydraulic diameters estimations, one for the patterns of MCHS-0 and MCHS-2 due to the solid fin as in equation (9a), and the second for other patterns due to porous fin as in equation (9b). They are estimated according to the following formula [30]

$$D_h = 4 \frac{A}{P} = 2 \frac{H \frac{W}{2}}{(H + \frac{W}{2})} = \frac{H W}{(H + \frac{W}{2})} \quad (9a)$$

While for the patterns having porous fins

$$D_h = 2 \frac{H W}{(H + W)} \quad (9b)$$

where A and P are the cross-sectional area of the flow and wetted perimeter of the channel, respectively. The H and W are the channel height and the width of a single channel and fin, respectively. According to the last equation, the velocity of the patterns having solid fins differs from the patterns having porous fins. The turbulence intensity (I) is estimated by [39]

$$I = \frac{0.16}{\sqrt[8]{Re}} \quad (10)$$

The friction factor is estimated based on the pressure drop across the microchannel according to the velocity of the fluid is [10]

$$f = \frac{2 \Delta p D_h}{L \rho u_m^2} \quad (11)$$

The local convection heat transfer coefficient and the local Nusselt number are defined as [10]

$$h_z = \frac{q L W}{A_c [T_{z,w} - T_{z,f}]} \quad (12)$$

$$Nu_z = \frac{h_z D_h}{\gamma_f} \quad (13)$$

where q , A_c , $T_{z,w}$, $T_{z,f}$, and k_f represent, respectively, the heat flux at the substrate bottom surface, the contact surface area of water and aluminum wall for a single microchannel, the local conduction wall temperature, local bulk fluid temperature, and the thermal conductivity of the fluid. It is necessary to be mentioned that W is the width of the computational domain taken in this study.

The average Nusselt number is obtained by

$$Nu = \frac{1}{L} \int_0^L Nu_z \cdot dz \quad (14)$$

The JF factor is defined as [10, 11]

$$JF = \frac{\left(\frac{Nu}{Nu_o}\right)}{\left(\frac{f}{f_o}\right)^{1/3}} \quad (15)$$

where the subscript (o) refers to the traditional MCHS (solid fin-fluid zone).

The smaller temperature difference between the maximum and minimum temperature of the bottom of the MCHS substrate means higher temperature uniformity. Thus, the main characteristics of the temperature uniformity are the temperature difference and the

temperature distribution on the whole bottom surface of the substrate. The last is characterized by the mean square deviation of the bottom surface temperature. Therefore, a non-dimensional evaluative parameter TU is proposed to carry out a comparison between the patterns investigated here. The formula of TU is [40]

$$TU = \frac{T_{max} - T_{min}}{T_{avg}^2} \left[\frac{1}{n} \sum_{i=1}^n (T_i - T_{avg})^2 \right]^{0.5} \quad (16)$$

where T_{max} , T_{min} , and T_{avg} are the maximum, minimum, and average temperature of the substrate bottom surface, respectively. T_i is the temperature of a point on the surface, n is the number of those points which are picked uniformly. The term in the blank on the right side of the above equation represents the mean square deviation of the surface temperature. Lower TU means higher temperature uniformity.

7. Results and discussion

In the current study, the traditional flat plate-fin microchannel heat sink is developed by using metallic porous media in several forms as illustrated in the previous figures (Figure 2 and 3); porous media fins with fluid core, solid fins with porous media core, porous media attached to the substrate, and fluid core upper the porous media, porous media fins having a varied cross-sectional area with y-axis and fluid core, and porous media fins having a varied cross-sectional area with z-axis with the fluid core. The goal of this investigation is to enhance the dissipation of heat generation from the processors to the ambient keeping the size of the heat sink constant. The purpose of this study is to improve heat dissipation from the processor to the environment while keeping the size of the heat sink constant. The new and novel heat sink design proposed here achieves significant and unexpected results when compared to conventional ones, and the new design can open a wide door to the industry for modifying the speed of processors more and more while keeping the temperature of electrical components below the critical temperature. The results obtained in this study are depicted and interpreted in the following sections.

7.1. Uniform cross-sectional area of the fins heat sink

In this section, the patterns of MCHS-0, MCHS-1, MCHS-2, MCHS-3, and MCHS-4 are investigated. The volume of each zone is kept constant except the last one for showing the effect of increasing the volume of the porous media on the hydraulic and thermal performance of the MCHS.

The results of the Nusselt number of the four proposed designs of the heat sink with the traditional one over different values of Reynolds numbers are depicted in Figure 7(A). It can be seen that the thermal performance of MCHS-0 is so low and does not match the high-speed of the processors produced nowadays. The Nusselt number is significantly and unexpectedly increased in the proposed designs, and this augmentation grows with increasing Re number. The Nusselt number rises considerably in the MCHS-1 pattern. This is owing to the area of the convection heat transfer between the fluid and the solid edges of the porous media which is greater than that between the fluid and solid-fin surface. In addition, the length of the fluid path passing through the porous matrix is longer than that when the solid fin is used. A longer path means a larger time required for the coolant to reach the

outlet of the channel, and then further heat can be absorbed by the fluid. Moreover, the reattachment and redevelopment of the thermal boundary layer between the fluid and solid edges of the porous matrix could greatly enhance the heat transfer rate. The heat is absorbed from the substrate by the porous fin by conduction and then dissipated away by the coolant by convection. Therefore, further heat can be dissipated keeping the heat sink size constant. The pattern of MCHS-2 shows a greater increase in the Nusselt number. This is due to the fact that convection heat transfer occurs in two places: between the fluid and solid fins and between the fluid and porous medium domains. In addition, the area of the contact between the solid fin and porous media with the upper surface of the substrate increases in this design. An additional enhancement in the Nusselt number is obtained in the pattern of MCHS-3. As it is well-known, the porous media absorbs the heat from the substrate more than the pure fluid. Thus, in this case, the heat is transferred from the substrate by conduction, then through the porous fin by both conduction and convection, and eventually to the fluid by convection. The conduction between the porous media and the channel bottom surface is doubled. Therefore, the constant area between the porous fin base and the heat sink substrate is greater in this pattern compared to others. This design could increase the heat absorption by the porous fin. A slight enhancement in the Nusselt number is also monitored in the pattern of MCHS-4 compared to MCHS-3. From this small improvement, it can be said that no great heat dissipation can be obtained by further increases in the porous media volume, and then no more economical benefit can be received. The last design has a double volume of porous medium compared to the others in which the porous fin and porous zone are used.

The flow characteristics represented by the friction factor are depicted with Re number for the five patterns of the MCHS as shown in Figure 7(B). The traditional pattern exhibits the lowest frictional loss which is generally decreased with the increase of the Re number. This is also because the pure-fluid channel has low flow resistance compared to that using porous media. The patterns of MCHS-1 and MCHS-3 show higher frictional losses compared to the traditional one, while their friction factors are close to each other. The last two designs show the same frictional losses approximately because they have the same cross-sectional area (normal to the flow direction) for both porous fin and fluid zone. The MCHS-2 has a greater friction factor, which may be explained by the presence of the solid fin (which reduces the cross-sectional area of the fluid flow) and the flow resistance generated by the porous media. It can be said that during the flow of the fluid through the porous matrix, the solid edges of the porous media restrict the fluid flow and plays as obstacles in the flow channel. Nevertheless, the MCHS-4 provides the highest frictional losses among the other patterns due to filling the whole zone above the heat sink substrate by porous media.

The representation of the flow characteristics in terms of friction factor in the present study is not adequate unless the pressure drop along the heat sink is also highlighted for a comprehensive understanding of the flow mechanism as seen in Figure 7(C). It can be seen that the pattern of MCHS-1 and MCHS-3 exhibits the same pressure drop and their pressure drop is lower than the MCHS-0. It can be attributed to the fact that the wetted perimeter of the flow is doubled compared to the traditional one in which

the fluid velocity is lower at the corresponding Reynolds number. It can be also seen that the MCHS-4 has a pressure loss similar to that of the traditional one approximately, while a significant and tremendous increase in the pressure drop is monitored in the pattern of MCHS-2. Although the wetted perimeter of the fluid flow is small due to the use of solid fin, the pressure increases due to the flow resistance caused by the porous media zone. Thus, if the pressure drop in the MCHS is a key role, the last pattern must be avoided.

The judgment of choosing the optimal pattern cannot be made unless the hydraulic-thermal performance is illustrated in terms of the JF factor. These results are illustrated in Figure 7(D) with different values of the Re number. It is worth to be mentioned here that the hydraulic-thermal performance of the proposed patterns is compared to the traditional one. It can be seen that the maximum JF observed is for the pattern of MCHS-1, in which the JF equals 9.5 due to a high increase in the Nusselt number compared to a moderate increase in the frictional loss. More considerable enhancement in the JF is observed in the pattern of MCHS-2 owing to the conduction through the solid fin and the solid edges of the porous media and also owing to the increase in the convection heat transfer area between the fluid and the solid. The MCHS-3 shows the highest JF factor due to the great Nusselt number enhancement accomplished with a low increase in the friction factor. This enhancement in the JF reduces when the MCHS-4 is used due to remarkable improvement in the friction factor with an enhancement in Nusselt number close to that of MCHS-3.

From the above results obtained, it can be encouraged that when thermal performance is a key role in the MCHS design, MCHS-4 is recommended. If the frictional loss plays an important role, the MCHS-3 can be counseled, as the highest JF obtained in this pattern is 15.6 at $Re = 3000$. This pattern can be also advised for designers whose hydraulic-thermal performance is the target. Economically, the amount of the porous fin material requirement is lower than that of the solid fin. Based on the equation of the effective density of the porous media which can be written as[22]

$$\rho_{\text{eff}} = (1 - \epsilon)\rho_s + \epsilon\rho_f \quad (17)$$

The reduction in the mass of the fin material is 58.68% when the solid fin is replaced by the porous one. Due to higher thermal effectiveness and material saving and a lower material requirement, the designers are encouraged for implementing the metal foam fins in their new MCHS designs.

At $Re = 3000$, the contours of the temperature distribution of the MCHS-0 are illustratively shown in Figure 8(A). It is explicitly observed that this pattern exhibits a big hot spot through the whole volume of the substrate and the solid fin temperature ranged from 300 K at the beginning of the fin tip up to 352 K at the bottom of the substrate. A great temperature drop is obtained when the porous fin is used instead of the solid one as shown in Figure 8(B). The most volume of the fin is cold and its temperature ranges from 300 K to 312 K. Moreover, the beginning of the substrate is colder compared to the traditional one, while the maximum temperature of the substrate bottom is still around 352 K. A significant and unexpected temperature gradient is monitored in the pattern of MCHS-2 as illustrated in Figure 8(C). Although

the fin almost has a low temperature (300 K – 300.8 K), most of the substrate domain is green (i.e., 301 K–301.9 K). It is worth to be mentioned that the maximum temperature of the solid wall is around 302.7 K. Figure 8(D) shows that the whole volume of the fin is cold (300 K–300.9 K) and most of the half volume of the substrate is below 302.8 K. In addition, the spot of hot temperature

(i.e., 304.1 K) is only at the downstream end of the substrate (at the bottom only). The pattern of MCHS-4 is explored as shown in Figure 8(E) in which higher temperature is recorded (303.8 K) at the downstream bottom of the substrate and most of the rest of the domain is less than 302.3 K.

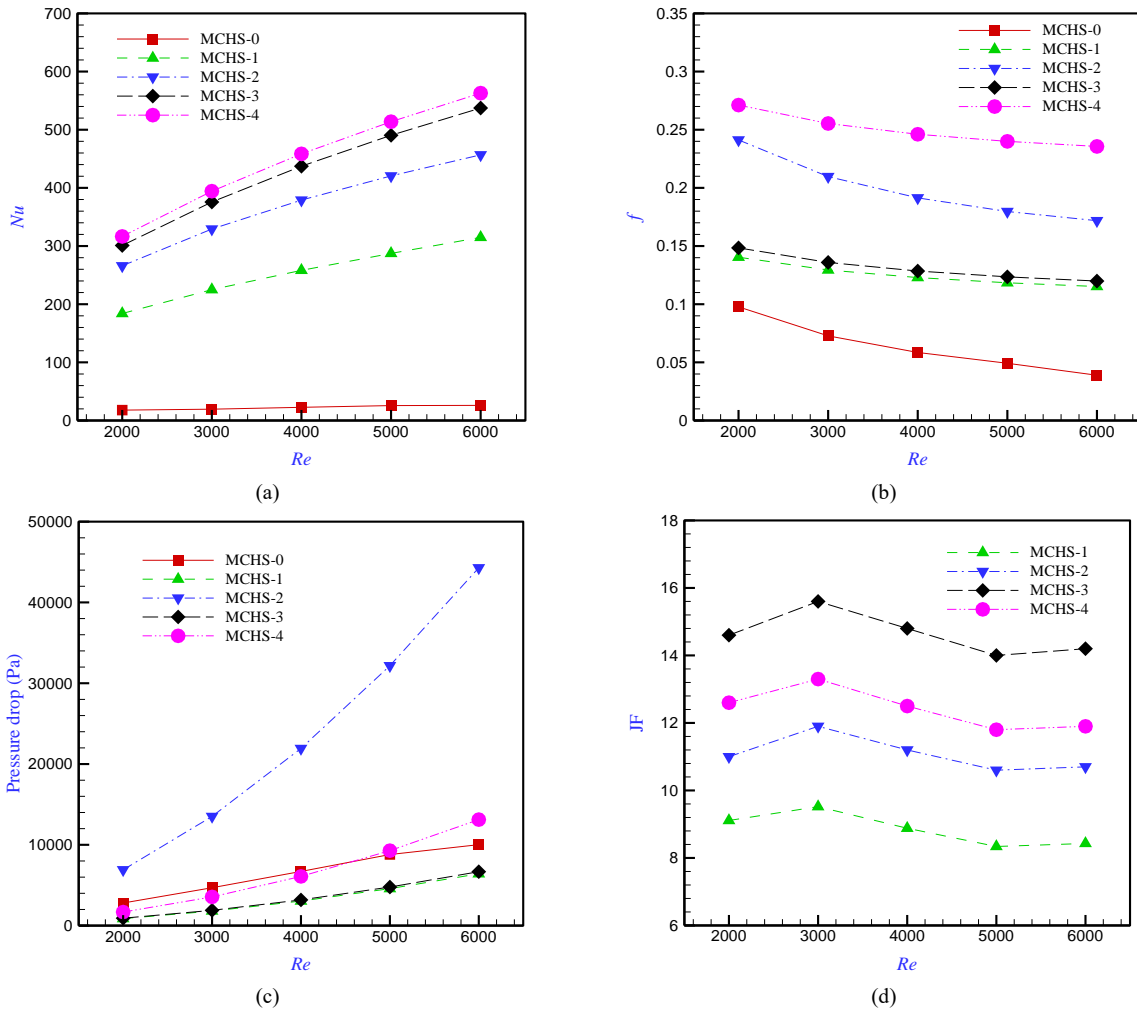


Figure 7. Comparison of the different MCHS patterns over the range of Re number; (A) Nusselt number, (B) friction factor, (C) pressure drop, and (D) JF factor.

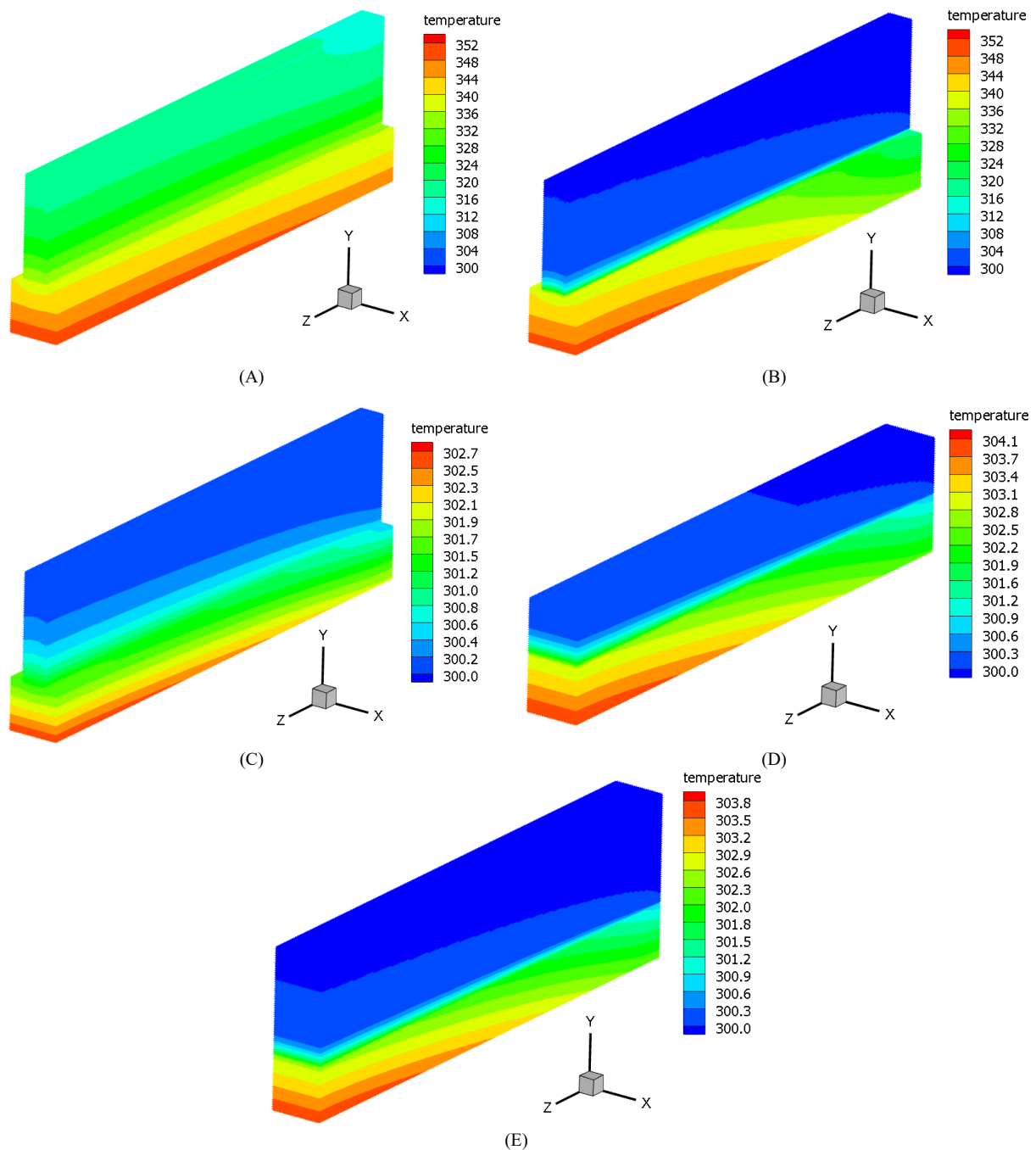


Figure 8. Contours of temperature distribution for (A) MCHS-0, (B) MCHS-1, (C) MCHS-2, (D) MCHS-3, and (E) MCHS-4.

7.2. Variable cross-sectional area of the porous fins with the y-axis

In this section, the pattern of MCHS-1 is explored here. Variable vertical cross-sectional areas of the porous fin are investigated keeping the total volume of the porous media zone constant. The length of the bottom side and topsides of the porous fin is; 0.5 mm and 0.5 mm, 0.7 mm and 0.3 mm, 0.8 mm and 0.2 mm, and finally 1.0 mm and 0.0 mm as illustratively shown in Figure 9(A)–(C), respectively.

The results of the Nusselt number with Re number for several patterns of the porous fin are displayed in Figure 9(A). The results show that the uniform cross-section porous fin provides Nu number from 184 to 314 at the lowest and highest value of Re number, respectively. This

result is the same as that shown in the previous section (7.1). When the length of the porous fin bottom is increased in the x-direction, the quantity of heat transported by conduction from the substrate to the porous fin grows, the Nusselt number is dramatically increased. This increment in the Nu number enhances with increasing the Re number. It can be said here that increasing the bottom-side length and decreasing the top-side length of the porous fin could cause higher conductive heat transfer between the fin and substrate in which the fin temperature increases due to the further heat absorbed. Thus, higher convective heat transfer occurs between the fluid and porous fin due to a large temperature difference between them. Due to the convection heat transfer between the coolant and the porous fin, the temperature of the porous fin decreases away from the wall, and this decrease in the temperature

reduces the effectiveness of the porous fin. Conclusively, the longest bottom side and zero top side porous fin (i.e., $a = 1.0$ mm and $b = 0.0$ mm) outperforms the traditional cross-sectional area of the porous fin in terms of heat transfer.

It can be also observed that the friction factor of the traditional and uniform cross-section porous fin is the lowest among all the proposed patterns as seen in Figure 9(B). However, all the other patterns provide a slight increase in the friction factor and their results are close to each other. It can be concluded that the frictional losses increase with increasing the tip angle of the cross-sectional area of the flow due to the thickening of the hydraulic boundary layer at the tip. In general, the friction factor decreases with increasing the Re number.

The results JF factor reveal that when the tip of the porous fin decreases, the JF factor increases monotonically and the results of all proposed patterns outperform the results of traditional uniform cross-sectional area porous fin as shown in Figure 9(C). The maximum JF factor obtained here is 15.9 for the last pattern shown in the figure legend. Therefore, for designing the MCHS with optimal hydraulic-thermal performance, the zero-tip length porous fin is recommended in which a wide door can be

opened for manufacturing ultra-high-speed electronic processors.

The contours of the temperature gradient of the MCHS-1 with a cross-sectional area of 0.5 mm \times 0.5 mm keeping the height constant are shown in Figure 10(A) and interpreted in the formal contours drawing. Figure 10(B) displays that when the bottom length of the fin is enlarged to be 0.7 mm and the tip length is reduced to 0.3 mm, the maximum temperature is remarkably dropped to 304.4 K. More temperature reduction is observed when the fin bottom length is enlarged to be 0.8 mm and 1.0 mm, as shown in Figure 10(C) and (D), respectively. It can be concluded that when the fin bottom width increases, the conduction area between the fin and substrate increases, and then more heat is transferred by the fin. This heat is dissipated from the fin to the fluid by convection. This convection heat transfer occurs greatly close to the bottom of the flow channel and reduces with y -direction. In that case, there is no need to keep the cross-sectional area of the fin constant with y -direction as the effectiveness of the fin reduces. These proposed patterns do not lower the quantity of fin material used, but rather change the design of the fins only when the heat transfer is significantly improved.

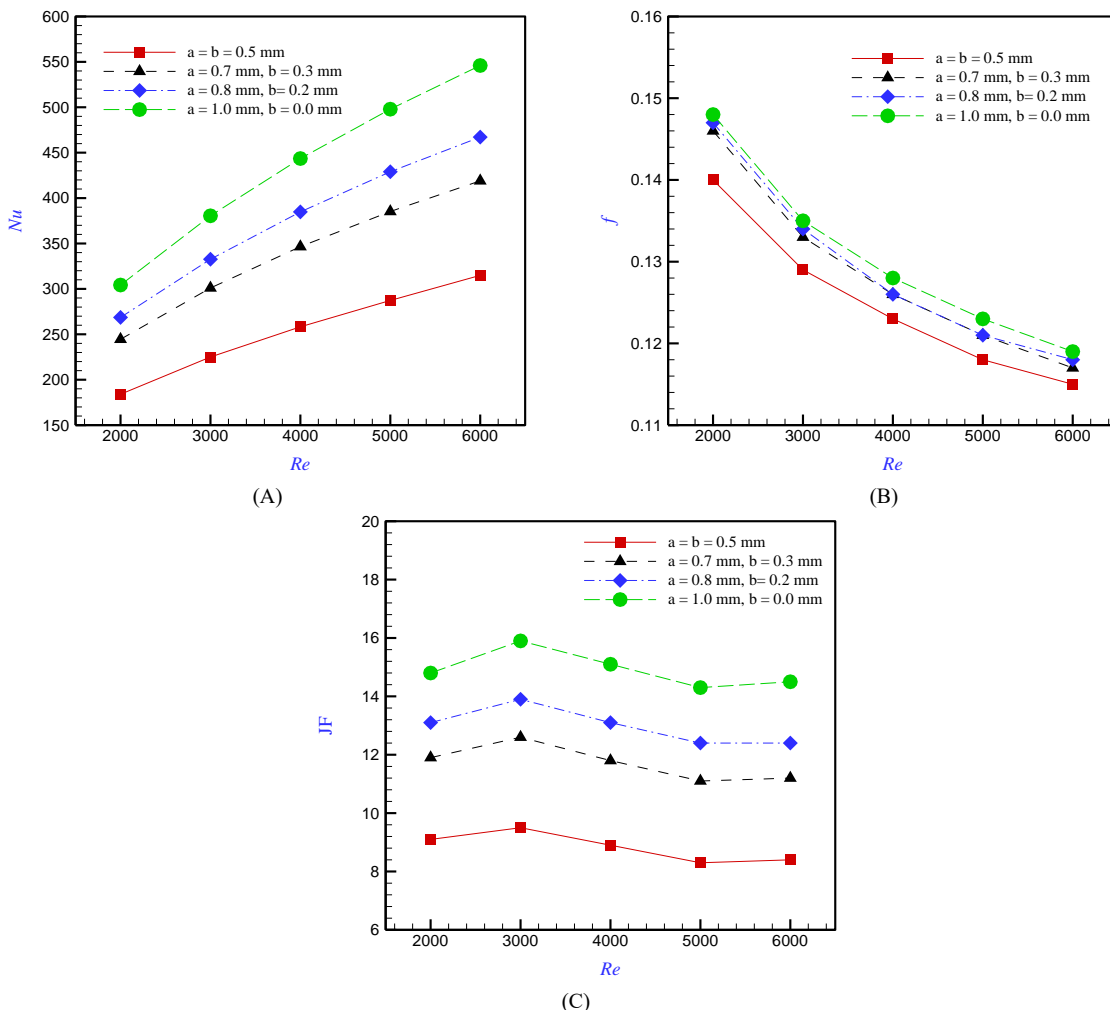


Figure 9. Effect of cross-sectional area varying with y -direction of MCHS-5 pattern on (A) the Nusselt number, (B) friction factor, and (C) JF factor.

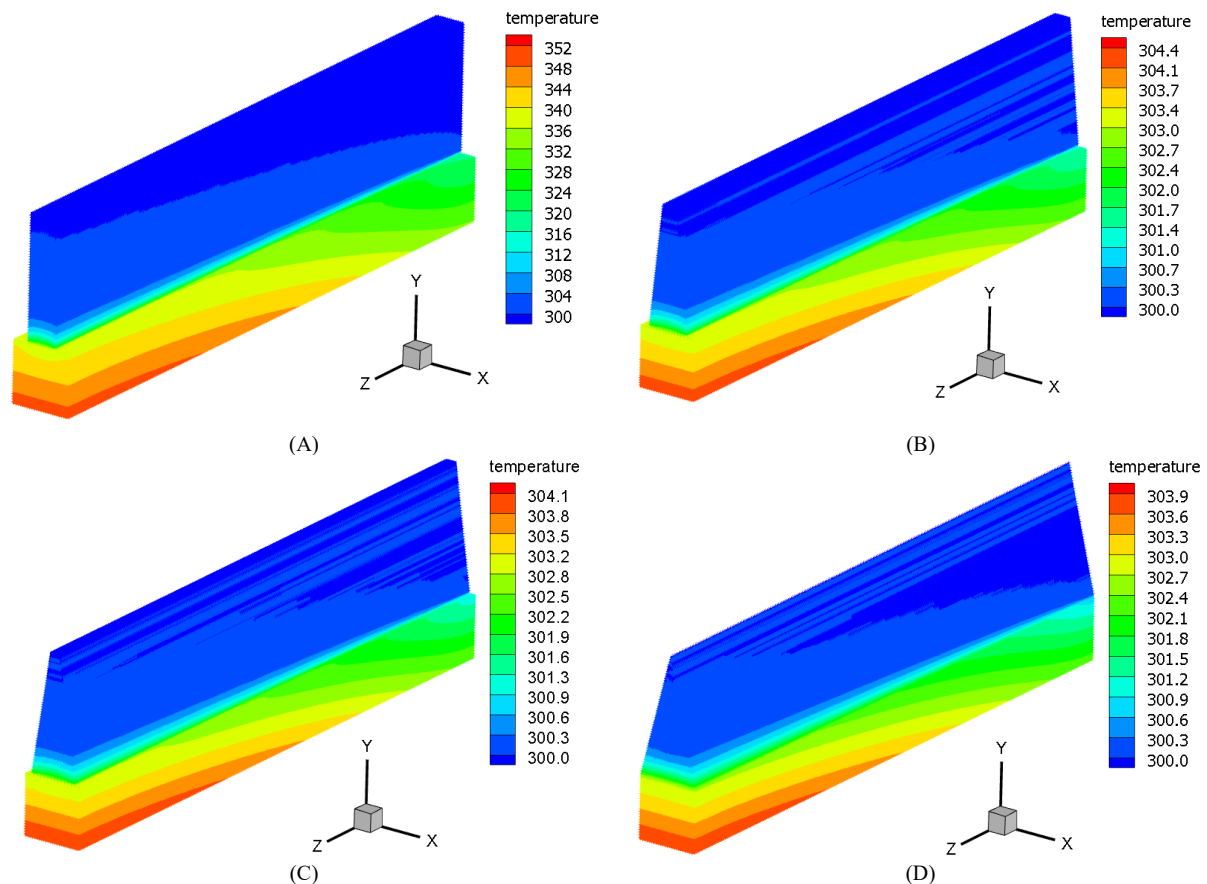


Figure 10. Contours of temperature distribution of the MCHS-5 pattern; (A) 0.5 mm, 0.5 mm, (B) 0.7 mm, 0.3 mm, (C) 0.8 mm, 0.2 mm, and (D) 1.0 mm, 0.0 mm, at $Re = 3000$.

7.3. Variable cross-sectional area of the porous fin with the z-axis

After studying the effect of varying the cross-sectional area with the y-axis, now the effect of varying the cross-sectional area with the longitudinal flow direction is investigated. It is worthy to be mentioned that the total volume of the porous fin is the same in both proposed designs and equal to the volume of the traditional porous fin volume.

The results of the Nusselt number infer that the MCHS-6 provides a lower Nusselt number than the MCHS-1 as shown in Figure 11(A). On the contrary, the MCHS-7 shows a significant increase in the Nusselt number compared to the aforementioned two patterns. It can be interpreted as the wall temperature of the upper surface of the substrate is high at the leading edge of the channel and decreases with the axial flow direction. Therefore, great heat absorption occurs at the beginning of the channel. Hence, there is no need to add more porous material downstream of the channel. Furthermore, both the MCHS-8 and MCHS-9 designs have seen a significant increase in the Nusselt number. Their heat dissipation is very similar, especially as the Reynolds number increases. Conclusively, the pattern of MCHS-8 and MCHS-9 have the optimal thermal performance compared to other patterns.

The lowest friction factor is observed for the MCHS-1 because the flow channel has a small flow resistance

along the axial flow direction (uniform cross-sectional area for the fluid zone) as shown in Figure 11(B). A higher friction factor is displayed for the MCHS-6 due to the smallest drag force at the channel inlet because of the sharp leading edge of the metal foam fin and gradually increases with the axial direction. In contrast, the friction factor of the MCHS-7 is slightly higher than the MCHS-6 because the cross-sectional area of the flow is filled with the porous media at the channel inlet in which the drag force is in its highest value. But the flow resistance decreases with the axial flow direction owing to the reduction in the cross-sectional area of the porous fin and increasing the cross-section of the fluid zone. The friction factor of pattern MCHS-8 is exactly the same as that of MCHS-7, but its Nusselt number is significantly higher. Further frictional losses are observed when the MCHS-9 is used due to the large drag force of the frontal area of the porous fin at the leading edge of the channel. In addition, the viscosity effect at the viscous sublayer in this pattern is higher than that in the MCHS-7 (as they have the same frontal area at the leading edge of the channel) and consequently greater frictional force is observed.

For a fully comprehensive picture of the hydraulic-thermal performance of these three different patterns, the JF factor is also depicted in Figure 11(C). The great value of the JF for the pattern of MCHS-6 is explicitly seen, particularly at low values of Re number, but it is lower than that of the MCHS-1. Further JF enhancement is noticed when the MCHS-7 is applied in which a huge amount of heat dissipation with a slight increase in the frictional loss

is carried out. A significant and unexpected enhancement in the JF factor is obtained in both MCHS-8 and MCHS-9. Therefore and conclusively, for the same volume of the porous fin, the engineers are encouraged to use the MCHS-8 or MCHS-9 when the Nusselt number is the vital key, and MCHS-8 when the friction plays an important role, and MCHS-8 or MCHS-9 when JF is the target, as the processor speed could be increased dramatically.

Figure 12(A) illustrates the contours of temperature distribution of the MCHS-1. This thermal behavior is explained in the formal contours figure. When the porous fin volume is kept constant, the cubic domain of the fin (MCHS-1) is replaced with a tetrahedral one having an apex-angle at the upstream end of the flow channel (MCHS-6) as seen in Figure 12(B). This design is proposed owing to its lower drag force in which the frictional loss in its lowest values. However, the temperature distribution is opposite as the highest temperature is observed at the leading edge of the substrate, and the temperature drops with the axial length.

The whole fin domain is cold and lower than 301 K. The opposite behavior is observed with the MCHS-7 as the coldest spot of the substrate is at the leading edge and the hottest is at the downstream end of the base, see Figure 12(C). It can be attributed that the hot spot substrate occurs under the low-amount material of porous fin in which the conduction is low as well. More temperature drop is observed when the pattern MCHS-8, see Figure 12(D), is used as the maximum temperature recorded is 303.8 K. Nevertheless, the maximum temperature in the MCHS-9, see Figure 12(E), is greater than the last pattern, 304.0 K, the electronic cooling by using the pattern of MCHS-9 is the optimal choice because the region of the hot spot in the last pattern is smaller and the cold region is larger. This pattern could offer better wall temperature uniformity. By looking at these contours, it can be concluded that the apex-angle of the fin can be also adjustable and investigated for obtaining uniform substrate base temperature.

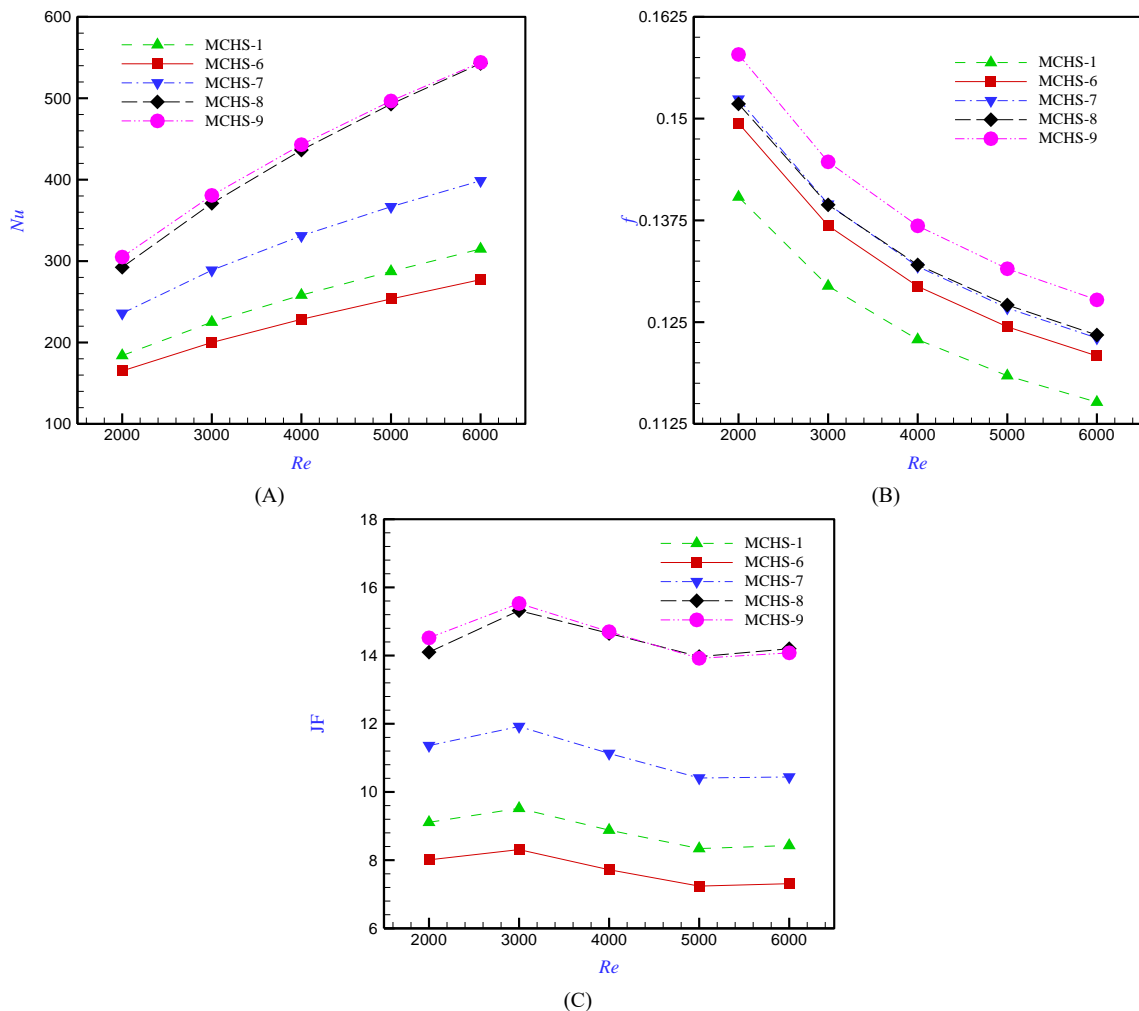


Figure 11. Comparison between the uniform and non-uniform cross-sectional area of the fin with z-direction (A) Nusselt number, (B) friction factor, and (C) JF.

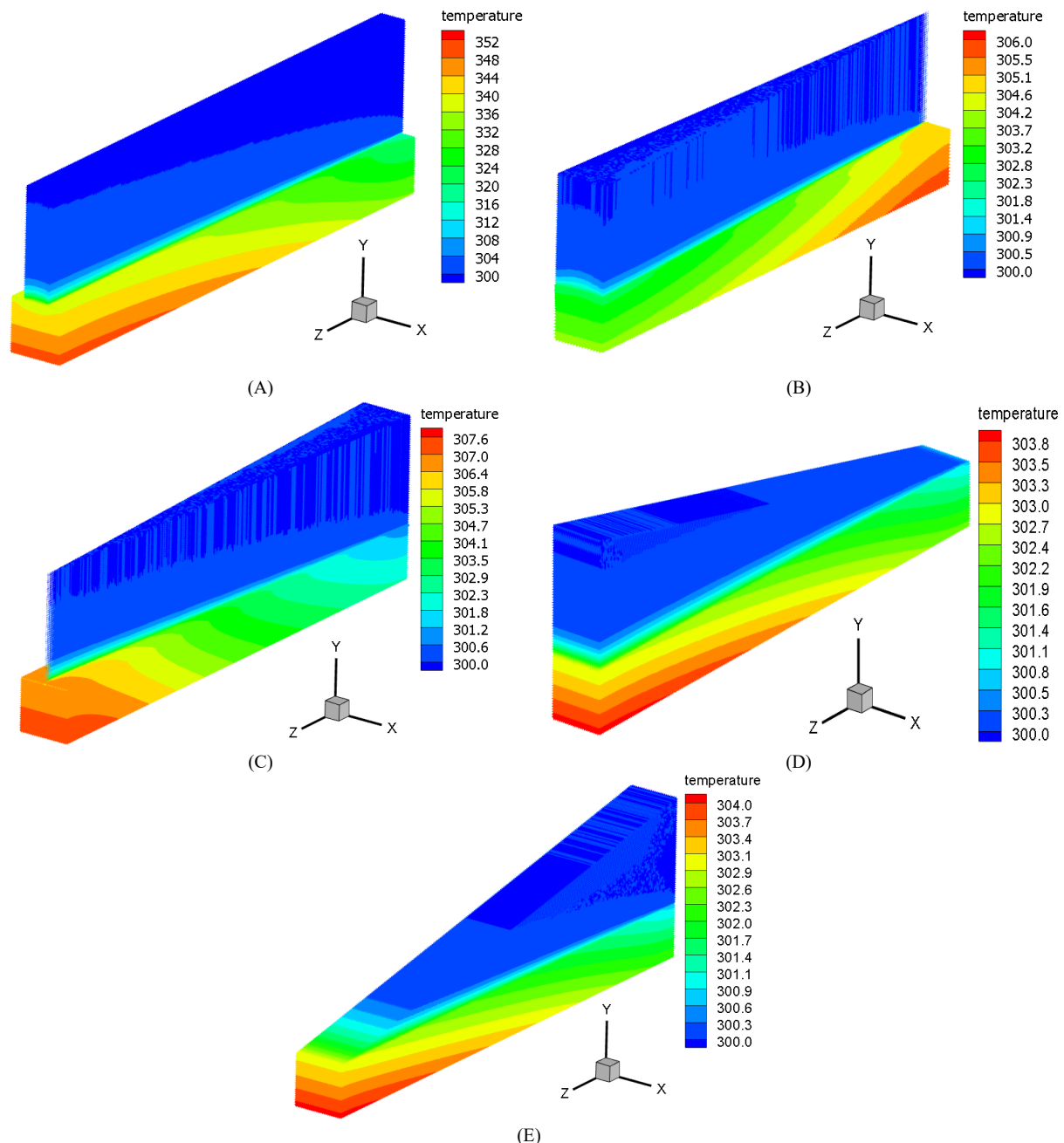


Figure 12. Contours of the temperature distribution of (A) MCHS-1, (B) MCHS-6, (C) MCHS-7, (D) MCHS-8, and (E) MCHS-9, at $Re = 3000$.

7.4. Uniformity of the wall temperature

The heat sink temperature plays an important role to protect the electronic components working below the critical temperature and increase the reliability. Therefore, the axial distribution of the temperature at the centerline of the channel bottom surface is depicted at $Re = 3000$. Figure 13(A) indicates that the MCHS-2, MCHS-3, and MCHS-4 layouts give the lowest heat sink base temperature. They also have a modest temperature variation between the upstream and downstream ends of the substrate. It is necessary to say that the MCHS-0 shows a very high wall temperature of the substrate. In addition, the pattern of MCHS-1 shows an exponential increase in the wall temperature and it shows the largest temperature difference although it provides a great heat dissipation in

comparison with the others. The pattern of MCHS-2 provides the smallest temperature difference compared to the others. When the parameters a and b are varied, all of these patterns exhibit a very small temperature difference concerning the constant cross-sectional area of the porous fin with the y-axis as shown in Figure 13(B). Precisely, the pattern of $a = 1.0$ mm and $b = 0.0$ mm shows the optimal trend. Furthermore, both the MCHS-6 and MCHS-7 display a significantly low difference in the temperature between the beginning and end of the substrate in comparison with the traditional porous fin as shown in Figure 13(C). Further study is carried out to evaluate the temperature uniformity using the non-dimensional parameter TU as shown in Figure 13(D) for three Reynolds numbers; 2000, 4000, and 6000. The smaller TU, the more temperature uniformity. It is necessary to say that the right y-axis is particular for the MCHS-1 due to its very

high TU values compared to other patterns. These high TU values can be attributed to the lower fluid velocity compared to the cases of the solid fins because the porous fin zone is included in the estimation of the hydraulic diameter at the corresponding Re number. It also emphasizes that the pattern of the MCHS-2 has the superiority of the temperature uniformity. Moreover, the TU decreases with increasing the Re number. The UT of

the patterns MCHS-6 to MCHS-9 is depicted in Figure 13(E) and also compared with the pattern of MCHS-1. As explained before, MCHS-1 has a high value of the TU and a large difference with Re . A lower value and smaller difference of TU are obtained by the pattern of MCHS-7 whilst a great TU is observed for other cases (i.e., MCHS-6, -8, and -9).

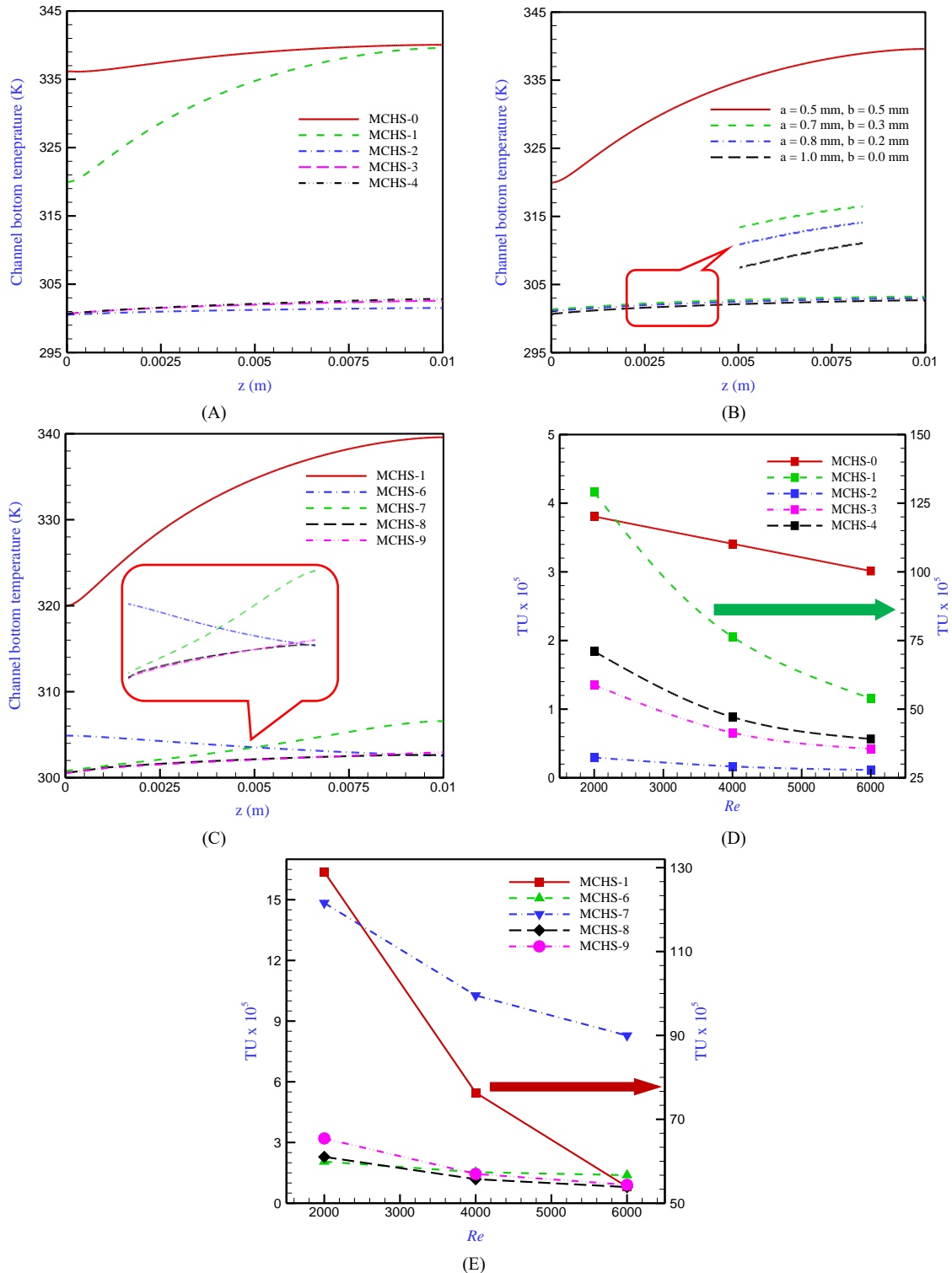


Figure 13. Temperature uniformity of the channel bottom (A) uniform cross-sectional area fin patterns, (B) MCHS-5, (C) variable cross-sectional area with z-axis at $Re = 3000$, (D) UT of MCHS-0 to -4, and (E) UT of MCHS-1 and MCHS-6 to -9.

Conclusions

In this paper, a three-dimensional computational simulation is carried out for enhancing the hydraulic and thermal performance of plate-fin MCHS using metal foam inserts over a range of Reynolds numbers from 2000 to 6000. Several new MCHS patterns are proposed considering the constant and variable cross-sectional area of the porous fin. The insert of porous media instead of the solid or fluid zone of the MCHS exhibits, in general, a significant enhancement in the Nusselt number accomplished with a moderate increase in the friction factor. The conclusions drawn from the predicted results can be summarized as follows:

1. The maximum increase in the Nusselt number and friction factor observed in the constant cross-sectional area of the porous fin is 20.66 times and 3.08 times, respectively, at $Re = 6000$ for the MCHS-3 compared to the traditional pattern. Besides, the optimal JF obtained is 15.65 at $Re = 3000$.
2. A tremendous enhancement in the Nusselt number (21.0 times) with a small increase in the friction factor (3.06 times) is observed for MCHS-5 (i.e., $a = 1.0$ mm, $b = 0.0$ mm) at $Re = 6000$, with respect to the traditional one. The maximum JF is 15.87 at $Re = 3000$ for the same pattern.
3. For the MCHS-9, a great improvement in the Nusselt number is revealed about 20.93 times at $Re = 6000$ associated with an insignificant increase in the friction factor of 3.29 times compared to the baseline one. Whilst it provides a JF of 15.53 at $Re = 3000$.
4. More enhancement in the Nusselt number (21.65 times) with additional frictional loss (6.06 times) is seen when the volume of the porous media is doubled (i.e., MCHS-4) in comparison with the traditional one, while the maximum JF factor is 11.87.
5. All proposed patterns of the MCHS exhibit a great temperature uniformity compared to the traditional fin design (MCHS-0). The optimal wall temperature uniformity (TU) observed is for the pattern of MCHS-2.

In general, all patterns that have variable cross-sectional areas of the porous fin with the vertical or axial direction provide significantly better thermal performance, hydraulic-thermal performance, and wall temperature uniformity compared to the constant cross-sectional fin area.

References

- [1] D.B. Tuckerman, R.F.W. Pease, High-performance heat sinking for VLSI, *IEEE Electron. Device Lett.* 2 (1981) 126–129.
- [2] X.-Y. Li, Sh.-L. Wang, X.-D. Wang, T.-H. Wang, Selected porous-ribs design for performance improvement in double-layered microchannel heat sinks, *International Journal of Thermal Sciences* 137 (2019) 616–626.
- [3] Ghahremannezhad, H. Xu, M.A. Nazari, M.H. Ahmadi, K. Vafai, Effect of porous substrates on thermohydraulic performance enhancement of double layer microchannel heat sinks, *International Journal of Heat and Mass Transfer* 131 (2019) 52–63.
- [4] T.-H. Wang, H.-Ch. Wu, J.-H. Meng, W.-M. Yan, Optimization of a double-layered microchannel heat sink with semi-porous-ribs by multi-objective genetic algorithm, *International Journal of Heat and Mass Transfer* 149 (2020) 119217.
- [5] S.T. Kadam, R. Kumar, Twenty first century cooling solution: microchannel heat sinks, *International Journal of Thermal Science* 85 (2014) 73–92.
- [6] S. Lu, K. Vafai, A comparative analysis of innovative microchannel heat sinks for electronic cooling, *International Communications in Heat and Mass Transfer* 76 (2016) 271–284.
- [7] N.H. Naquiuddin, L.H. Saw, M.C. Yew, F. Yusof, T.C. Ng, M.K. Yew, Overview of micro-channel design for high heat flux application, *Renewable and Sustainable Energy Review* 82 (2018) 901–914.
- [8] L. Chuan, X.-D. Wang, T.-H. Wang, W.-M. Yan, Fluid flow and heat transfer in microchannel heat sink based on porous fin design concept, *International Communications in Heat and Mass Transfer* 65 (2015) 52–57.
- [9] Ch.-H. Chen, Forced convection heat transfer in microchannel heat sinks, *International Journal of Heat and Mass Transfer* 50 (2007) 2182–2189.
- [10] Y. Li, L. Gong, M. Xu, Y. Joshi, Hydraulic and Thermal Performances of Metal Foam and Pin Fin Hybrid Heat Sink, *Applied Thermal Engineering*, 166 (2020) 114665.
- [11] H. Arasteh, R. Mashayekhi, M. Goodarzi, S.H. Motaharpour, M. Dahari, D. Toghraie, Heat and fluid flow analysis of metal foam embedded in a double-layered sinusoidal heat sink under local thermal non-equilibrium condition using nanofluid, *Journal of Thermal Analysis and Calorimetry*, <https://doi.org/10.1007/s10973-019-08168-x>.
- [12] S.Q. Hussien, A.A. Farhan, The effect of metal foam fins on the thermohydraulic performance of a solar air heater, *International Journal of Renewable Energy Research*, 9 (2) (2019) 840–847.
- [13] M.A. Nima, A.M. Ali, Numerical study of heat transfer enhancement for a flat plate solar collector by adding metal foam blocks, *Journal of Engineering*, 23(12) (2017) 13–32.
- [14] Heydari, M. Mesgarpour, M.R. Gharib, Experimental and Numerical Study of Heat Transfer and Tensile Strength of Engineered Porous Fins to Estimate the Best Porosity, *Jordan Journal of Mechanical and Industrial Engineering* 14(3) (2020) 339–348.
- [15] T.-Ch. Hung, Y.-X. Huang, W.-M. Yan, Thermal performance analysis of porous-microchannel heat sinks with different configuration designs, *International Journal of Heat and Mass Transfer* 66 (2013) 235–243.
- [16] R. Singh, A. Akbarzadeh, M. Mochizuki, Sintered porous heat sink for cooling of high-powered microprocessors for server applications, *International Journal of Heat and Mass Transfer* 52 (2009) 2289–2299.
- [17] T.C. Hung, W.M. Yan, Thermal performance enhancement of microchannel heat sinks with porous metallic medium, *Numerical Heat Transfer Part A: Application* 63 (9) (2013) 666–686.
- [18] Z.M. Wan, J. Liu, K.L. Su, X.H. Hu, S.S. M, Flow and heat transfer in porous micro heat sink for thermal management of high power LEDs, *Microelectronics Journal* 42 (2011) 632–637.
- [19] T.-Ch. Hung, Y.-X. Huang, W.-M. Yan, Thermal performance of porous microchannel heat sink: Effects of enlarging channel outlet, *International Communications in Heat and Mass Transfer* 48 (2013) 86–92.
- [20] H.R. Seyf, M. Layeghi, Numerical analysis of convective heat transfer from an elliptic pin fin heat sink with and without metal foam insert, *Journal of Heat Transfer ASME*, 132 (2010) 071401-1.

- [21] S.S. Feng, J.J. Kuang, T. Wen, T.J. Lu, K. Ichimiya, An experimental and numerical study of finned metal foam heat sinks under impinging air jet cooling, *International Journal of Heat and Mass Transfer* 77 (2014) 1063–1074.
- [22] M. Siavashi, H. Rasam, A. Izadi, Similarity solution of air and nanofluid impingement cooling of a cylindrical porous heat sink, *Journal of Thermal Analysis and Calorimetry*, <https://doi.org/10.1007/s10973-018-7540-0>.
- [23] Deng, Y. Qiu, Ch.N. Kim, An improved porous medium model for microchannel heat sinks, *Applied Thermal Engineering* 30 (2010) 2512–2517.
- [24] V. Yerramalle, B. Premachandran, P. Talukdar, Numerical investigation of the performance of interface conditions for fluid flow through a partially filled porous channel, *Thermal Science and Engineering Progress* 20 (2020) 100628.
- [25] Arbak, N. Dukhan, Performance and heat transfer measurements in asymmetrically-heated metal foam cooled by water, *Thermal Science and Engineering Progress* 20 (2020) 100688.
- [26] H.j. Xu, Ch. Zhao, K. Vafai, Analysis of double slip model for a partially filled porous microchannel—An exact solution, *European Journal of Mechanics / B Fluids* 68 (2018) 1–9.
- [27] H.J. Xu, L. Gong, C.Y. Zhao, Y.H. Yang, Z.G. Xu, Analytical considerations of local thermal non-equilibrium conditions for thermal transport in metal foams, *International Journal of Thermal Sciences* 95 (2015) 73–87.
- [28] A.K. AL-Migdady, A.M. Jawarneh, A.Kh. Ababneh, H.N. Dalgamoni, Numerical investigation of the cooling performance of PCM-based heat sinks integrated with metal foam insertion, *Jordan Journal of Mechanical and Industrial Engineering* 15(2) (2021) 191 – 197.
- [29] Alshare, W. Al-Kouz, S. Kiwan, A. Al-khalidi, M. Hader, Computational modeling of gaseous flow and heat transfer in a wavy microchannel, *Jordan Journal of Mechanical and Industrial Engineering* 10(1) (2016) 75–83.
- [30] Th.L. Bergman, A.S. Lavine, F.P. Incropera, D.P. DeWitt. *Fundamentals of Heat and Mass Transfer*. 7th edition, New York: J. Wiley, 2002.
- [31] X. Chen, F. Tavakkoli, K. Vafai, Analysis and characterization of metal foam-filled double-pipe heat exchangers, *Num. Heat Trans., Part A: App.: Int. J. Comput. Methodol.* 68 (2015) 1031–1049.
- [32] Alazmi, K. Vafai, Analysis of fluid flow and heat transfer interfacial conditions between a porous medium and a fluid layer, *International Journal of Heat and Mass Transfer* 44 (2001) 1735–1749.
- [33] Amiri, K. Vafai, T.M. Kuzay, Effect of boundary conditions on non-darcian heat transfer through porous media and experimental comparisons, *Numerical Heat Transfer J. Part A* 27 (1995) 651–664.
- [34] K. Vafai, R. Thiyagaraja, Analysis of flow and heat transfer at the interface region of a porous medium, *International Journal of Heat and Mass Transfer* 30 (1987) 1391–1405.
- [35] K. Vafai, Convective flow and heat transfer in variable porosity media, *Journal of Fluid Mechanics* 25 (1984) 233–259.
- [36] K. Vafai, C. Tien, Boundary and inertia effects on flow and heat transfer in porous media, *International Journal of Heat and Mass Transfer* 24 (1981) 195–203.
- [37] Hsu, P. Cheng, Thermal dispersion in a porous medium, *International Journal of Heat and Mass Transfer* 33 (1990) 1587–1597.
- [38] J. Wang, H. Kong, Y. Xu, J. Wu, J., Experimental investigation of heat transfer and flow characteristics in finned copper foam heat sinks subjected to jet impingement cooling, *Applied Energy* 241 (2019) 433–443.
- [39] Fluent A. 12.0 theory guide. Ansys Inc; 2009.
- [40] Z. He, Y. Yan, Sh. Feng, X. Li, Zh. Yang, Numerical study of thermal enhancement in a micro-heat sink with ribbed pin-fin arrays, *Journal of Thermal Analysis and Calorimetry* 143 (2021) 2163–2177.